

## Research Article

# Thermo-Magneto-Solutal Squeezing Flow of Nanofluid between Two Parallel Disks Embedded in a Porous Medium: Effects of Nanoparticle Geometry, Slip and Temperature Jump Conditions

M. G. Sobamowo , A. T. Akinshilo, and A. A. Yinusa

*Department of Mechanical Engineering, University of Lagos, Akoka-Yaba, Lagos, Nigeria*

Correspondence should be addressed to M. G. Sobamowo; [mikegbeminiyi@gmail.com](mailto:mikegbeminiyi@gmail.com)

Received 13 December 2017; Revised 25 March 2018; Accepted 10 April 2018; Published 3 June 2018

Academic Editor: Joseph Virgone

Copyright © 2018 M. G. Sobamowo et al. This is an open access article distributed under the Creative Commons Attribution License, which permits unrestricted use, distribution, and reproduction in any medium, provided the original work is properly cited.

The various applications of squeezing flow between two parallel surfaces such as those that are evident in manufacturing industries, polymer processing, compression, power transmission, lubricating system, food processing, and cooling amongst others call for further study on the effects of various parameters on the flow phenomena. In the present study, effects of nanoparticle geometry, slip, and temperature jump conditions on thermo-magneto-solutal squeezing flow of nanofluid between two parallel disks embedded in a porous medium are investigated, analyzed, and discussed. Similarity variables are used to transform the developed governing systems of nonlinear partial differential equations to systems of nonlinear ordinary differential equations. Homotopy perturbation method is used to solve the systems of the nonlinear ordinary differential equations. In order to verify the accuracy of the developed analytical solutions, the results of the homotopy perturbation method are compared with the results of the numerical method using the shooting method coupled with the fourth-order Runge–Kutta, and good agreements are established. Through the approximate analytical solutions, parametric studies are carried out to investigate the effects of nanoparticle size and shape, Brownian motion parameter, nanoparticle parameter, thermophoresis parameter, Hartmann number, Lewis number and pressure gradient parameters, slip, and temperature jump boundary conditions on thermo-solutal and hydromagnetic behavior of the nanofluid. This study will enhance and advance the understanding of nanofluidics such as energy conservation, friction reduction, and micromixing of biological samples.

## 1. Introduction

The study of squeezing flow of fluid between two parallel surfaces has received considerable and appreciable attentions in the last few decades due to its various industrial and biological applications. These applications are evident in manufacturing industries, polymer processing, compression, power transmission, lubricating system, food processing, and cooling amongst others. In the past efforts to analyze fluid flow behavior between two parallel surfaces under the influences of various flow, fluid, and external properties, Mustafa et al. [1] presented an analysis of heat and mass transfer between parallel plates undergoing unsteady squeezing fluid

flow while in the previous year, Hayat et al. [2] studied the squeezing flow behavior of a second grade fluid between parallel disk under the influence of presence of magnetic field. In an earlier work, Domairry and Aziz [3] applied the homotopy perturbation method to investigate the effects of suction and injection on magnetohydrodynamic squeezing flow of fluid between parallel disks. Also, Siddiqui et al. [4] investigated squeezing flow of viscous fluid between two parallel plates under the unsteady flow condition. In the same year, Rashidi et al. [5] examined the unsteady squeezing flow between parallel plates and presented different approximate analytical solutions. Three years later, Khan and Aziz [6] submitted a study on the flow of nanofluid between parallel

plates due to natural convection. In a further work in the same year, the same authors [7] analyzed a double-diffusive natural convective boundary-layer fluid flow through porous media saturated with nanofluid while in an earlier work, Kuznetsov and Nield [8] studied the flow of nanofluid between two parallel plates considering the effect of the natural convective boundary layer. Hashimi et al. [9] presented stimulating exploration of analytical solutions for the study of squeezing flow of nanofluid. Most of the above reviews have been limited to the analysis of squeezing flow under no slip and no temperature jump boundary conditions. However, when flow system characteristic size is small or at a low flow pressure, the assumption of no slip boundary condition becomes insufficient and inadequate in predicting the flow behavior of the fluid under such scenario. Therefore, additional boundary conditions are required to adequately predict the low flow pressure or low system characteristics size. Moreover, it has been established that in many cases of fluid and flow problems, such as polymeric liquids, thin film problems, nanofluids, rarefied fluid problems, fluids containing concentrated suspensions, and flow on multiple interfaces, slip condition prevails at the boundary of the flow [10–21]. Such slip boundary condition was first initiated by Navier [22] upon which other researchers have built their analysis [10, 11]. Therefore, in recent years, the effects of slip effect on fluid flow have been considered by many researchers [12–21] due to its significance to most practical fluid flow situations. Furthermore, the effect of stretching sheet wall problem adopting natural convective boundary conditions was investigated by Yao et al. [23], Kandasamy et al. [24], and Makinde and Aziz [25]. More works on parametric studies of the flow process can be found in [26–34]. Additionally, analyses of magnetohydrodynamic flow in the porous medium have been presented in various works [35–50] while various studies of magneto-nanofluid flow have also been presented in the past works [51–68].

The development of analytical solutions through some approximate analytical methods such as the Adomian decomposition method, homotopy analysis method, variation iteration method, and differential transformation method for the flow process has been semianalytic in procedures and applications. In the earlier efforts to develop total analytic methods for solving nonlinear equations, different perturbation methods such as regular, singular, and homotopy perturbation methods have been applied. However, among these methods, the traditional perturbation methods such as methods of regular and singular perturbations require the inclusion of a small parameter in the governing differential equations for the approximate analytical solution(s) to be realized for the governing differential equations. In the class of the newly developed approximate analytical methods for solving nonlinear equations, the homotopy perturbation method has been considered to be relatively simple with fewer requirements for mathematical rigour or skill. The homotopy perturbation method (HPM) gives highly accurate analytical solutions without the need for small perturbation parameters as required in traditional perturbations [69–73]. The results of

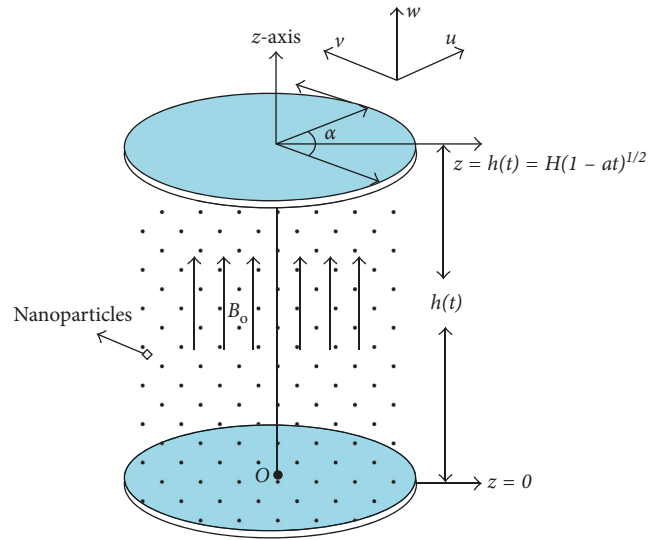


FIGURE 1: The squeezing flow of nanofluid between the parallel circular plates.

HPM are completely reliable and physically realistic. Unlike the other approximate analytical methods, the HPM does not involve the search for a particular value that will satisfy the end boundary condition. Furthermore, to the best of our knowledge, there is no study where the thermal-diffusion and diffusion-thermal of magnetohydrodynamic squeezing unsteady flow of nanofluid between two parallel disks embedded in a porous medium under the influences of different nanoparticle geometries, slip and temperature jump conditions are analyzed. Therefore, in this work, the homotopy perturbation method is used to study the effects of nanoparticle geometry, slip, and temperature jump conditions on thermo-magneto-solutal squeezing flow of nanofluid between two parallel disks embedded in a porous medium. The obtained analytical solutions are used to investigate the effects of the Brownian motion parameter, thermophoresis parameter, Hartmann number, Lewis number and pressure gradient parameters, slip, and temperature jump boundary conditions on fluid behavior of the nanofluid.

## 2. Model Development and Analytical Solutions

Consider an axisymmetrical flow of nanofluid through two parallel disks as shown in Figure 1. The upper disk is moving towards the stationary lower disks under a uniform magnetic field strength applied perpendicular to disks as depicted in Figure 1. The fluid conducts electrical energy as it flows unsteadily under the influence of magnetic force field. It is assumed that the fluid structure is everywhere in thermodynamic equilibrium and the plate is maintained at constant temperature.

The details of the governing equation and non-dimensional parameters have been described by Hashimi et al. [9] and Das et al. [20] which can be introduced under the stated assumptions in the previous studies as

$$\begin{aligned}
\frac{\partial u}{\partial r} + \frac{u}{r} + \frac{\partial w}{\partial z} &= 0, \\
\frac{\partial u}{\partial t} + u \frac{\partial u}{\partial r} + w \frac{\partial u}{\partial z} &= -\frac{1}{\rho_{\text{nf}}} \cdot \frac{\partial p}{\partial r} + \nu_{\text{nf}} \left( \frac{\partial^2 u}{\partial r^2} + \frac{\partial^2 u}{\partial z^2} + \frac{1}{r} \cdot \frac{\partial u}{\partial r} - \frac{u}{r^2} \right) - \frac{\sigma_{\text{nf}} B^2(t) u}{\rho_{\text{nf}}} - \frac{\nu_{\text{nf}} u}{K_p}, \\
\frac{\partial w}{\partial t} + u \frac{\partial w}{\partial r} + w \frac{\partial w}{\partial z} &= -\frac{1}{\rho_{\text{nf}}} \cdot \frac{\partial p}{\partial z} + \nu_{\text{nf}} \left( \frac{\partial^2 w}{\partial r^2} + \frac{\partial^2 w}{\partial z^2} + \frac{1}{r} \cdot \frac{\partial w}{\partial r} \right) - \frac{\nu_{\text{nf}} w}{K_p}, \\
\frac{\partial T}{\partial t} + u \frac{\partial T}{\partial r} + w \frac{\partial T}{\partial z} &= \alpha_{\text{nf}} \left( \frac{\partial^2 T}{\partial r^2} + \frac{1}{r} \cdot \frac{\partial T}{\partial r} + \frac{\partial^2 T}{\partial z^2} \right) + \tau_{\text{nf}} \left[ D_B \left( \frac{\partial c}{\partial r} \cdot \frac{\partial T}{\partial r} + \frac{\partial c}{\partial z} \cdot \frac{\partial T}{\partial z} \right) + \frac{D_T}{T_m} \left\{ \left( \frac{\partial T}{\partial r} \right)^2 + \left( \frac{\partial T}{\partial z} \right)^2 \right\} \right], \\
\frac{\partial c}{\partial t} + u \frac{\partial c}{\partial r} + w \frac{\partial c}{\partial z} &= D_{B,\text{nf}} \left( \frac{\partial^2 c}{\partial r^2} + \frac{1}{r} \cdot \frac{\partial c}{\partial r} + \frac{\partial^2 c}{\partial z^2} \right) + \frac{D_T}{T_m} \left( \frac{\partial^2 T}{\partial r^2} + \frac{1}{r} \cdot \frac{\partial T}{\partial r} + \frac{\partial^2 T}{\partial z^2} \right),
\end{aligned} \tag{1}$$

where

$$\begin{aligned}
\rho_{\text{nf}} &= (1 - \phi) \rho_f + \phi \rho_s, \\
\mu_{\text{nf}} &= \frac{\mu_f}{(1 - \phi)^{2.5}}, \\
\sigma_{\text{nf}} &= \sigma_f \left[ 1 + \frac{3 \{ (\sigma_s / \sigma_f) - 1 \} \phi}{\{ (\sigma_s / \sigma_f) + 2 \} \phi - \{ (\sigma_s / \sigma_f) - 1 \} \phi} \right], \\
\alpha_{\text{nf}} &= \frac{(\rho C_p)_{\text{nf}}}{k_{\text{nf}}}, \\
(\rho C_p)_{\text{nf}} &= (1 - \phi) (\rho C_p)_f + \phi (\rho C_p)_s, \\
k_{\text{nf}} &= k_f \left[ \frac{k_s + (m - 1) k_f - (m - 1) (k_f - k_s) \phi}{k_s + (m - 1) k_f + (k_f - k_s) \phi} \right].
\end{aligned} \tag{2}$$

The appropriate initial and boundary conditions given as

$$\begin{aligned}
u = 0, \quad w = 0, \quad T = T_o, \quad c = c_o, \quad \text{at } t = 0, \quad 0 \leq z \leq H, \\
u = -\beta_1 \frac{\partial u}{\partial z}, \quad w = \frac{w_0}{\sqrt{1 - \alpha t}}, \quad T = -\gamma_1 \frac{\partial T}{\partial z} + T_w, \quad c = c_w, \quad z = 0, \\
u = -\beta_1 \frac{\partial u}{\partial z}, \quad w = w_h \left( \frac{\partial h}{\partial t} \right), \quad T = \gamma_1 \frac{\partial T}{\partial z} + T_h, \quad c = c_h, \\
\text{at } z = h(t).
\end{aligned} \tag{3}$$

Using the following dimensionless quantities and similarity transformations,

$$\begin{aligned}
A &= \frac{w_0}{\alpha H}, \\
\beta &= \frac{\beta_1}{H \sqrt{1 - \alpha t}},
\end{aligned}$$

$$\begin{aligned}
\gamma &= \frac{\gamma_1}{H \sqrt{1 - \alpha t}}, \\
Nt &= \frac{\tau D_B (T_w - T_h)}{\nu}, \\
Nb &= \frac{\tau D_B (k_w - k_h)}{\nu}, \\
Le &= \frac{\nu}{D_B}, \\
Pr &= \frac{\nu}{\alpha}, \\
M &= HB_0 \sqrt{\frac{\sigma}{\mu}}, \\
Da &= \frac{K}{H}, \\
C &= \left( \frac{\alpha H}{\mu_f \nu_f} \right) \left( \frac{\partial p}{\partial z} \right), \\
S &= \frac{\alpha H^2}{2\nu}, \\
\varphi &= \frac{c - c_h}{c_w - c_h}, \\
\theta &= \frac{T - T_h}{T_w - T_h}, \\
w &= \frac{\alpha H}{2 \sqrt{1 - \alpha t}} f(\eta), \\
u &= \frac{\alpha r}{2(1 - \alpha t)} f'(\eta),
\end{aligned}$$

$$\begin{aligned}
\eta &= \frac{z}{H\sqrt{1-\alpha t}}, \\
\tau &= \frac{(\rho c)_p}{(\rho c)_f}, \\
K_1 &= (1-\phi) + \phi \left\{ \frac{\rho_s}{\rho_f} \right\}, \\
K_2 &= (1-\phi) + \phi \left\{ \frac{(\rho C_p)_s}{(\rho C_p)_f} \right\}, \\
K_3 &= \left[ \frac{k_s + (m-1)k_f - (m-1)(k_f - k_s)\phi}{k_s + (m-1)k_f + (k_f - k_s)\phi} \right], \\
B_1 &= \left[ \frac{(\sigma_s + (m-1)\sigma_f) + (m-1)(\sigma_s - \sigma_f)\phi}{(\sigma_s + (m-1)\sigma_f) - (m-1)(\sigma_s - \sigma_f)\phi} \right].
\end{aligned} \tag{4}$$

The dimensionless equations are given as

$$\begin{aligned}
\frac{d^4 f}{d\eta^4} - SK_1(1-\phi)^{2.5} \left( \eta \frac{d^3 f}{d\eta^3} + 3 \frac{d^2 f}{d\eta^2} + f \frac{df}{d\eta} - 2 \frac{df}{d\eta} \cdot \frac{d^3 f}{d\eta^3} \right) \\
- M^2 B_1(1-\phi)^{2.5} \frac{d^2 f}{d\eta^2} - \frac{1}{Da} B_1(1-\phi)^{2.5} \frac{d^2 f}{d\eta^2} = C,
\end{aligned} \tag{5}$$

$$\begin{aligned}
\frac{d^2 \theta}{d\eta^2} + \frac{PrSK_2}{K_3} \left( 2f \frac{d\theta}{d\eta} - \eta \frac{d\theta}{d\eta} \right) \\
+ \frac{Pr}{K_3(1-\phi)^{2.5}} \left( Nb \frac{d\theta}{d\eta} \cdot \frac{d\phi}{d\eta} + Nt \left( \frac{d\theta}{d\eta} \right)^2 \right) = 0,
\end{aligned} \tag{6}$$

$$\frac{d^2 \phi}{d\eta^2} + LeSK_1(1-\phi)^{2.5} (2f - \eta) \frac{d\theta}{d\eta} + \frac{Nt}{Nb} \cdot \frac{d^2 \phi}{d\eta^2} = 0. \tag{7}$$

And the dimensionless boundary conditions are given as

$$\begin{aligned}
f(0) &= A, \frac{df(0)}{d\eta} \\
f(1) &= \frac{1}{2}, \\
\frac{df(1)}{d\eta} &= \beta \frac{d^2 f(1)}{d\eta^2}, \\
\theta(0) &= 1 - \gamma \frac{d\theta}{d\eta}, \\
\theta(1) &= \gamma \frac{d\theta}{d\eta}, \\
\phi(0) &= 0, \\
\phi(1) &= 0,
\end{aligned} \tag{8}$$

$$\begin{aligned}
\phi(0) &= 0, \\
\phi(1) &= 0,
\end{aligned} \tag{9}$$

where  $m$  in the above Hamilton Crosser's model in (4) is the shape factor, and its numerical values for different shapes are given in Table 1.

The physical and thermal properties of the basefluid and nanoparticles are given in Tables 2 and 3, respectively.

It should be noted that the shape factor  $m = 3/\psi$ , where  $\psi$  is the sphericity (the ratio of the surface area of the sphere and the surface area of the real particles with equal volumes). Sphericity of sphere, platelet, cylinder, laminar, and brick are 1.000, 0.526, 0.625, 0.185, and 0.811, respectively. Hamilton–Crosser's model becomes Maxwell–Garnett's model, when the shape factor of the nanoparticle is  $m = 3$ . SWCNTs represent single-walled carbon nanotubes.

### 3. Method of Solution by the Homotopy Perturbation Method

The comparative advantages and the provision of acceptable analytical results with convenient convergence and stability [69–73] coupled with total analytic procedures of the homotopy perturbation method compel us to consider the method for solving the system of nonlinear differential equations in (5)–(7).

*3.1. The Basic Idea of the Homotopy Perturbation Method.* In order to establish the basic idea behind the homotopy perturbation method, consider a system of nonlinear differential equations given as

$$A(U) - f(r) = 0, \quad r \in \Omega. \tag{10}$$

With the boundary conditions

$$B\left(u, \frac{\partial u}{\partial \eta}\right) = 0, \quad r \in \Gamma, \tag{11}$$

where  $A$  is a general differential operator,  $B$  is a boundary operator,  $f(r)$  is a known analytical function, and  $\Gamma$  is the boundary of the domain  $\Omega$ .

The operator  $A$  can be divided into two parts,  $L$  and  $N$ , where  $L$  is a linear operator and  $N$  is a nonlinear operator. Equation (10) can be therefore rewritten as follows:

$$L(u) + N(u) - f(r) = 0. \tag{12}$$

By the homotopy technique, a homotopy  $U(r, p) : \Omega \times [0, 1] \rightarrow R$  can be constructed, which satisfies

$$\begin{aligned}
H(U, p) &= (1-p)[L(U) - L(U_o)] \\
&+ p[A(U) - f(r)] = 0, \quad p \in [0, 1],
\end{aligned} \tag{13}$$

or

$$\begin{aligned}
H(U, p) &= L(U) - L(U_o) + pL(U_o) \\
&+ p[N(U) - f(r)] = 0.
\end{aligned} \tag{14}$$

In the above (13) and (14),  $p \in [0, 1]$  is an embedding parameter and  $u_0$  is an initial approximation of equation of (10), which satisfies the boundary conditions.

Also, from (13) and (14), one has

$$H(U, 0) = L(U) - L(U_0) = 0. \quad (15)$$

or

$$H(U, 0) = A(U) - f(r) = 0. \quad (16)$$

The changing process of  $p$  from zero to unity is just that of  $U(r, p)$  from  $u_0(r)$  to  $u(r)$ . This is referred to homotopy in topology. Using the embedding parameter  $p$  as a small parameter, the solutions of (13) and (14) can be assumed to be written as a power series in  $p$  as given in (17):

$$U = U_0 + pU_1 + p^2U_2 + \dots \quad (17)$$

It should be pointed out that of all the values of  $p$  are between 0 and 1, and  $p = 1$  produces the best result. Therefore, setting  $p = 1$ , results in the approximation solution of (9):

$$u = \lim_{p \rightarrow 1} U = U_0 + U_1 + U_2 + \dots \quad (18)$$

The basic idea expressed above is a combination of the homotopy and perturbation method. Hence, the method is called the homotopy perturbation method (HPM), which has eliminated the limitations of the traditional perturbation methods (regular and singular perturbation methods). On the other hand, this technique can have full advantages of the traditional perturbation techniques. The series (18) is convergent for most cases.

**3.2. Application of the Homotopy Perturbation Method to the Present Problem.** According to the homotopy perturbation method (HPM), one can construct an homotopy for (5)–(7) as

$$\begin{aligned} H_1(p, \eta) = (1-p) \left[ \frac{d^4 f}{d\eta^4} - C \right] + p \left[ \frac{d^4 f}{d\eta^4} - SK_1(1-\phi)^{2.5} \right. \\ \cdot \left( \eta \frac{d^3 f}{d\eta^3} + 3 \frac{d^2 f}{d\eta^2} + f \frac{df}{d\eta} - 2 \frac{df}{d\eta} \cdot \frac{d^3 f}{d\eta^3} \right) - M^2 B_1 \\ \cdot \left. (1-\phi)^{2.5} \frac{d^2 f}{d\eta^2} - \frac{1}{Da} B_1 (1-\phi)^{2.5} \frac{d^2 f}{d\eta^2} - C \right] = 0, \end{aligned} \quad (19)$$

$$\begin{aligned} H_2(p, \eta) = (1-p) \left[ \frac{d^2 \theta}{d\eta^2} \right] + p \left[ \frac{d^2 \theta}{d\eta^2} + \frac{PrSK_2}{K_3} \left( 2f \frac{d\theta}{d\eta} - \eta \frac{d\theta}{d\eta} \right) \right. \\ \left. + \frac{Pr}{K_3(1-\phi)^{2.5}} \left( Nb \frac{d\theta}{d\eta} \cdot \frac{d\phi}{d\eta} + Nt \left( \frac{d\theta}{d\eta} \right)^2 \right) \right] = 0, \end{aligned} \quad (20)$$

$$\begin{aligned} H_3(p, \eta) = (1-p) \left[ \frac{d^2 \phi}{d\eta^2} \right] + p \left[ \frac{d^2 \phi}{d\eta^2} + LeSK_1(1-\phi)^{2.5} \right. \\ \cdot \left. (2f - \eta) \frac{d\theta}{d\eta} + \frac{Nt}{Nb} \cdot \frac{d^2 \phi}{d\eta^2} \right] = 0. \end{aligned} \quad (21)$$

Taking power series of velocity, temperature, and concentration fields gives

$$f = f_0 + pf_1 + p^2f_2 + \dots, \quad (22)$$

$$\theta = \theta_0 + p\theta_1 + p^2\theta_2 + \dots, \quad (23)$$

$$\phi = \phi_0 + p\phi_1 + p^2\phi_2 + \dots \quad (24)$$

Substituting (22) into (19) yields

$$p^0: \frac{d^4 f_0}{d\eta^4}, \quad (25)$$

$$\begin{aligned} p^1: \frac{d^4 f_1}{d\eta^4} - M^2 B_1 (1-\phi)^{2.5} \frac{d^2 f_0}{d\eta^2} - \frac{1}{Da} B_1 (1-\phi)^{2.5} \frac{d^2 f_0}{d\eta^2} \\ - C - SK_1(1-\phi)^{2.5} \left( 3 \frac{d^2 f_0}{d\eta^2} + \eta \frac{d^3 f_0}{d\eta^3} \right. \\ \left. + f_0 \frac{df_0}{d\eta} - 2 \frac{df_0}{d\eta} \cdot \frac{d^3 f_0}{d\eta^3} \right), \end{aligned} \quad (26)$$

$$\begin{aligned} p^2: \frac{d^4 f_2}{d\eta^4} - \frac{d^2 f_1}{d\eta^2} M^2 B_1 (1-\phi)^{2.5} - \frac{1}{Da} B_1 (1-\phi)^{2.5} \frac{d^2 f_1}{d\eta^2} \\ - SK_1(1-\phi)^{2.5} \left( 3 \frac{d^2 f_1}{d\eta^2} + \frac{d^3 f_1}{d\eta^3} - \frac{df_0}{d\eta} \left( 2 \frac{df_1}{d\eta} - f_1 \right) \right. \\ \left. - \frac{df_1}{d\eta} \left( 2 \frac{df_0}{d\eta} - f_0 + 2 \right) \right), \\ \vdots \end{aligned} \quad (27)$$

The boundary conditions for (25)–(27) are

$$f_0(0) = A, \quad f_1(0) = 0, \quad f_2(0) = 0,$$

$$\frac{df_0(0)}{d\eta} = -\beta \frac{d^2 f_0(0)}{d\eta^2},$$

$$\frac{df_1(0)}{d\eta} = -\beta \frac{d^2 f_1(0)}{d\eta^2},$$

$$\frac{df_2(0)}{d\eta} = -\beta \frac{d^2 f_2(0)}{d\eta^2},$$

$$f_0(1) = \frac{1}{2}, \quad f_1(1) = 0, \quad f_2(1) = 0,$$

$$\frac{df_0(1)}{d\eta} = \beta \frac{d^2 f_0(1)}{d\eta^2},$$

$$\begin{aligned}\frac{df_1(1)}{d\eta} &= \beta \frac{d^2 f_1(1)}{d\eta^2}, \\ \frac{df_2(1)}{d\eta} &= \beta \frac{d^2 f_2(1)}{d\eta^2}.\end{aligned}\quad (28)$$

Substituting (23) into (20) yields

$$p^0: \frac{d^2 \theta_0}{d\eta^2}, \quad (29)$$

$$\begin{aligned}p^1: & \frac{d^2 \theta_1}{d\eta^2} - \frac{PrSK_2}{K_3} \left( \eta \frac{d\theta_0}{d\eta} - 2 \frac{d\theta_0}{d\eta} f_0 \right) + \frac{Pr}{K_3(1-\phi)^{2.5}} \\ & \cdot \left( Nb \frac{d\theta_0}{d\eta} \cdot \frac{d\phi_0}{d\eta} + Nt \left( \frac{d\theta_0}{d\eta} \right)^2 \right),\end{aligned}\quad (30)$$

$$\begin{aligned}p^2: & \frac{d^2 \theta_2}{d\eta^2} + \frac{PrSK_2}{K_3} \left( 2 \frac{d\theta_0}{d\eta} f_1 - \frac{d\theta_1}{d\eta} + 2 \frac{d\theta_1}{d\eta} f_0 \right) + \frac{Pr}{K_3(1-\phi)^{2.5}} \\ & \cdot \left( Nb \frac{d\theta_1}{d\eta} \cdot \frac{d\phi_0}{d\eta} + Nb \frac{d\theta_0}{d\eta} \cdot \frac{d\phi_1}{d\eta} + 2Nt \frac{d\theta_0}{d\eta} \cdot \frac{d\theta_1}{d\eta} \right), \\ & \vdots.\end{aligned}\quad (31)$$

The boundary conditions for (29)–(31) are

$$\begin{aligned}\theta_0(0) &= 1 - \gamma \frac{d\theta_0}{d\eta}, \\ \theta_1(0) &= -\gamma \frac{d\theta_1}{d\eta}, \\ \theta_2(0) &= -\gamma \frac{d\theta_2}{d\eta}, \\ \theta_0(1) &= \gamma \frac{d\theta_0}{d\eta}, \\ \theta_1(1) &= \gamma \frac{d\theta_1}{d\eta}, \\ \theta_2(1) &= \gamma \frac{d\theta_2}{d\eta}.\end{aligned}\quad (32)$$

Substituting (24) into (21) yields

$$p^0: \frac{d^2 \phi_0}{d\eta^2} + \left( \frac{Nt}{Nb} \cdot \frac{d^2 \theta_0}{d\eta^2} \right), \quad (33)$$

$$\begin{aligned}p^1: & \frac{d^2 \phi_1}{d\eta^2} + \left( \frac{Nt}{Nb} \cdot \frac{d^2 \phi_1}{d\eta^2} \right) \\ & - LeSK_1(1-\phi)^{2.5} \left( \eta \frac{d\theta_0}{d\eta} - 2 \frac{d\theta_0}{d\eta} f_0 \right),\end{aligned}\quad (34)$$

$$\begin{aligned}p^2: & \frac{d^2 \phi_2}{d\eta^2} + LeSK_1(1-\phi)^{2.5} \left( 2 \frac{d\theta_0}{d\eta} f_1 - \eta \frac{d\theta_1}{d\eta} + 2 \frac{d\theta_1}{d\eta} f_0 \right) \\ & + \left( \frac{Nt}{Nb} \cdot \frac{d^2 \theta_2}{d\eta^2} \right), \\ & \vdots.\end{aligned}\quad (35)$$

The boundary conditions for (33)–(35) are

$$\begin{aligned}\phi_0(0) &= 0, \\ \phi_1(0) &= 0, \\ \phi_2(0) &= 0, \\ \phi_0(1) &= 0, \\ \phi_1(1) &= 0, \\ \phi_2(1) &= 0.\end{aligned}\quad (36)$$

On solving (25), applying the boundary condition (28) gives

$$f_0 = A - \frac{(2A-1)\eta^3}{(6\beta-1)} + \frac{3(2A-1)\eta^2}{(12\beta-2)} - \frac{3\beta(2A-1)\eta}{(6\beta-1)}. \quad (37)$$

Also, on solving (29), applying the boundary condition (32) yields

$$\theta_0 = \frac{\eta}{(2\gamma-1)} + \frac{\gamma-1}{2\gamma-1}. \quad (38)$$

And the solution of (33), by applying the boundary condition (36) is

$$\phi_0 = 0. \quad (39)$$

On solving (26) and applying the boundary condition (28), one arrives at

$$\begin{aligned}
f_1 = \eta^4 & \left( \frac{C}{24} - \frac{SK_1(1-\phi)^{2.5}}{16} - \frac{A^2SK_1(1-\phi)^{2.5}}{8} + \frac{3ASK_1(1-\phi)^{2.5}}{16} - \frac{SK_1(1-\phi)^{2.5}(2A-1)^2}{48(6\beta-1)^2} \right. \\
& + \frac{(2A-1)(1-\phi)^{2.5}(12(M^2+(1/Da))B_1+20SK_1-10ASK_1)}{96(6\beta-1)} \left. \right) + \frac{C^{19}\eta^2}{2} + \frac{C^{20}\eta^3}{6} - \eta \left( \frac{C}{24} + \frac{C}{12} + \frac{C^{20}}{6} - \frac{29SK_1(1-\phi)^{2.5}}{480} \right) \\
& - \frac{7A^2SK_1(1-\phi)^{2.5}}{60} + \frac{43ASK_1(1-\phi)^{2.5}}{240} - \frac{53SK_1(1-\phi)^{2.5}(2A-1)^2}{10080(6\beta-1)^2} - \frac{8SK_1(1-\phi)^{2.5}-16ASK_1(1-\phi)^{2.5}(2A-1)}{3360(6\beta-1)} \\
& + \frac{57SK_1(1-\phi)^{2.5}-78ASK_1(1-\phi)^{2.5}(2A-1)}{1440(6\beta-1)^2} + \frac{(2A-1)(1-\phi)^{2.5}(12(M^2+(1/Da))B_1+20SK_1-10ASK_1)}{96(6\beta-1)} \\
& - \frac{(2A-1)(1-\phi)^{2.5}(24(M^2+(1/Da))B_1+122SK_1-64ASK_1)}{480(6\beta-1)} - \frac{(57SK_1(1-\phi)^{2.5}-78ASK_1(1-\phi)^{2.5})(2A-1)}{1440(6\beta-1)} \\
& - \frac{\eta^6(7SK_1(1-\phi)^{2.5}(2A-1)^2)}{96(6\beta-1)^2} + \frac{\eta^7(17SK_1(1-\phi)^{2.5}(2A-1)^2)}{336(6\beta-1)^2} - \frac{(2A-1)(8SK_1(1-\phi)^{2.5}-16ASK_1(1-\phi)^{2.5})}{3360(6\beta-1)} \\
& - \frac{\eta^8(17SK_1(1-\phi)^{2.5}(2A-1)^2)}{1120(6\beta-1)^2} + \frac{\eta^9(SK_1(1-\phi)^{2.5}(2A-1)^2)}{1008(6\beta-1)^2} + \eta^5 \left( \frac{SK_1(1-\phi)^{2.5}}{480} + \frac{A^2SK_1(1-\phi)^{2.5}}{120} \right. \\
& \left. - \frac{ASK_1(1-\phi)^{2.5}}{120} + \frac{5SK_1(1-\phi)^{2.5}(2A-1)^2}{96(6\beta-1)^2} - \frac{(2A-1)(1-\phi)^{2.5}(24(M^2+(1/Da))B_1+122SK_1-64ASK_1)}{480(6\beta-1)} \right). \tag{40}
\end{aligned}$$

On solving (30), applying the boundary condition in (32) gives

$$\begin{aligned}
\theta_1 = \frac{PrSK_2}{106K_3} \left( \frac{2A-1}{(\beta-1)(2\gamma-1)} \right) \eta^5 - \frac{PrSK_2}{4K_3} \left( \frac{2A-1}{(\beta-1)(2\gamma-1)} \right) \eta^4 + \frac{PrSK_2}{6K_3} \left( \frac{1-2\gamma-2A+4A\gamma}{(2\gamma-1)^2} \right) + \frac{PrSK_2}{6K_3} \left( \frac{2A-1}{(\beta-1)(2\gamma-1)} \right) \eta^3 \\
- \frac{PrSK_2}{60K_3} \left( \frac{2A-1}{(\beta-1)(2\gamma-1)} \right) \eta - \frac{PrNt}{K_3(1-\phi)^{2.5}2(2\gamma-1)^2} - \frac{PrSK_2}{6K_3} \frac{(1-2\gamma-2A+4A\gamma)}{2(2\gamma-1)^2}. \tag{41}
\end{aligned}$$

It can easily be shown that the solution of (34) after applying the boundary condition of (36) yields

$$\begin{aligned}
\varphi_1 = \frac{PrSK_2Nb}{K_3Nt} \left\{ \frac{\gamma(1-2A)}{5(6\beta-1)(2\gamma-1)^2} - \frac{(1-2A)\eta^5}{10(6\beta-1)(2\gamma-1)^2} + \frac{(1-2A)}{4(6\beta-1)(2\gamma-1)^2} - \frac{\gamma(1-2A)\eta^4}{2(6\beta-1)(2\gamma-1)^2} - \frac{\beta(1-2A)\eta^3}{(6\beta-1)(2\gamma-1)^2} \right. \\
+ \frac{(1-6\beta)(1-2A)}{(6\beta-1)(2\gamma-1)^2} - \frac{(1-2A-6\beta+12A\beta)\eta^2}{2(6\beta-1)(2\gamma-1)^2} - \frac{Nt(1-6\beta)\eta^2}{2S(6\beta-1)(2\gamma-1)^2} + \frac{\beta(1-2A)}{(6\beta-1)(2\gamma-1)^2} + \frac{(1-2A-6\beta+12A\beta)}{2(6\beta-1)(2\gamma-1)^2} \\
\left. + \frac{Nt(1-6\beta)}{2S(6\beta-1)(2\gamma-1)^2} - \frac{\gamma(1-6\beta)(1-2A)}{(6\beta-1)(2\gamma-1)^2} - \frac{\gamma(1-2A\beta)}{5(6\beta-1)(2\gamma-1)^2} + \frac{\gamma(1-2A\beta)\eta}{2(6\beta-1)(2\gamma-1)^2} \right\}. \tag{42}
\end{aligned}$$



In the same way,  $f_2(\eta)$ ,  $\theta_2(\eta)$ , and  $\phi_2(\eta)$  are (27), (31), and (35) are solved using the boundary conditions in (28), (32), and (36), respectively. Although the resulting solutions and the other subsequent solutions are too long to be shown

in this paper, they are included in the simulated results shown graphically in the results and discussion section.

Substituting (37) and (40) into the power series (22) yields

$$\begin{aligned}
 f(\eta) = & A - \frac{(2A-1)\eta^3}{(6\beta-1)} + \frac{3(2A-1)\eta^2}{(12\beta-2)} - \frac{3\beta(2A-1)\eta}{(6\beta-1)} + \eta^4 \left( \frac{C}{24} - \frac{SK_1(1-\phi)^{2.5}}{16} - \frac{A^2SK_1(1-\phi)^{2.5}}{8} + \frac{3ASK_1(1-\phi)^{2.5}}{16} \right. \\
 & - \frac{SK_1(1-\phi)^{2.5}(2A-1)^2}{48(6\beta-1)^2} + \frac{(2A-1)(1-\phi)^{2.5}(12(M^2+(1/Da))B_1+20SK_1-10ASK_1)}{96(6\beta-1)} \Bigg) \\
 & + \frac{C^{19}\eta^2}{2} + \frac{C^{20}\eta^3}{6} - \eta \left( \frac{C}{24} + \frac{C}{12} + \frac{C^{20}}{6} - \frac{29SK_1(1-\phi)^{2.5}}{480} \right) - \frac{7A^2SK_1(1-\phi)^{2.5}}{60} \\
 & + \frac{43ASK_1(1-\phi)^{2.5}}{240} - \frac{53SK_1(1-\phi)^{2.5}(2A-1)^2}{10080(6\beta-1)^2} - \frac{8SK_1(1-\phi)^{2.5}-16ASK_1(1-\phi)^{2.5}(2A-1)}{3360(6\beta-1)} \\
 & + \frac{57SK_1(1-\phi)^{2.5}-78ASK_1(1-\phi)^{2.5}(2A-1)}{1440(6\beta-1)^2} + \frac{(2A-1)(1-\phi)^{2.5}(12(M^2+(1/Da))B_1+20SK_1-10ASK_1)}{96(6\beta-1)} \\
 & - \frac{(2A-1)(1-\phi)^{2.5}(24(M^2+(1/Da))B_1+122SK_1-64ASK_1)}{480(6\beta-1)} \\
 & - \frac{(57SK_1(1-\phi)^{2.5}-78ASK_1(1-\phi)^{2.5})(2A-1)}{1440(6\beta-1)} - \frac{\eta^6(7SK_1(1-\phi)^{2.5}(2A-1)^2)}{96(6\beta-1)^2} + \frac{\eta^7(17SK_1(1-\phi)^{2.5}(2A-1)^2)}{336(6\beta-1)^2} \\
 & - \frac{(2A-1)(8SK_1(1-\phi)^{2.5}-16ASK_1(1-\phi)^{2.5})}{3360(6\beta-1)} - \frac{\eta^8(17SK_1(1-\phi)^{2.5}(2A-1)^2)}{1120(6\beta-1)^2} + \frac{\eta^9(SK_1(1-\phi)^{2.5}(2A-1)^2)}{1008(6\beta-1)^2} \\
 & + \eta^5 \left( \frac{SK_1(1-\phi)^{2.5}}{480} + \frac{A^2SK_1(1-\phi)^{2.5}}{120} - \frac{ASK_1(1-\phi)^{2.5}}{120} + \frac{5SK_1(1-\phi)^{2.5}(2A-1)^2}{96(6\beta-1)^2} \right. \\
 & \left. - \frac{(2A-1)(1-\phi)^{2.5}(24(M^2+(1/Da))B_1+122SK_1-64ASK_1)}{480(6\beta-1)} \right).
 \end{aligned} \tag{43}$$

Also, substituting (38) and (41) into the power series (23) gives

$$\begin{aligned}
 \theta(\eta) = & \frac{\eta}{(2\gamma-1)} + \frac{\gamma-1}{2\gamma-1} + \frac{PrSK_2}{106K_3} \left( \frac{2A-1}{(\beta-1)(2\gamma-1)} \right) \eta^5 - \frac{PrSK_2}{4K_3} \left( \frac{2A-1}{(\beta-1)(2\gamma-1)} \right) \eta^4 + \frac{PrSK_2}{6K_3} \left( \frac{1-2\gamma-2A+4A\gamma}{(2\gamma-1)^2} \right) \\
 & + \frac{PrSK_2}{6K_3} \left( \frac{2A-1}{(\beta-1)(2\gamma-1)} \right) \eta^3 - \frac{PrSK_2}{60K_3} \left( \frac{2A-1}{(\beta-1)(2\gamma-1)} \right) \eta - \frac{PrNt}{K_3(1-\phi)^{2.5}2(2\gamma-1)^2} - \frac{PrSK_2}{3K_3} \cdot \frac{(1-2\gamma-2A+4A\gamma)}{(2\gamma-1)^2} + \dots
 \end{aligned} \tag{44}$$



Similarly, substituting (39) and (42) into the power series (24) yields

$$\begin{aligned} \varphi(\eta) = \frac{\text{PrSK}_2Nb}{K_3Nt} \left\{ \frac{\gamma(1-2A)}{5(6\beta-1)(2\gamma-1)^2} - \frac{(1-2A)\eta^5}{10(6\beta-1)(2\gamma-1)^2} + \frac{(1-2A)}{4(6\beta-1)(2\gamma-1)^2} - \frac{\gamma(1-2A)\eta^4}{2(6\beta-1)(2\gamma-1)^2} - \frac{\beta(1-2A)\eta^3}{(6\beta-1)(2\gamma-1)^2} \right. \\ + \frac{(1-6\beta)(1-2A)}{(6\beta-1)(2\gamma-1)^2} - \frac{(1-2A-6\beta+12A\beta)\eta^2}{2(6\beta-1)(2\gamma-1)^2} - \frac{Nt(1-6\beta)\eta^2}{2S(6\beta-1)(2\gamma-1)^2} + \frac{\beta(1-2A)}{(6\beta-1)(2\gamma-1)^2} + \frac{(1-2A-6\beta+12A\beta)}{2(6\beta-1)(2\gamma-1)^2} \\ \left. + \frac{Nt(1-6\beta)}{2S(6\beta-1)(2\gamma-1)^2} - \frac{\gamma(1-6\beta)(1-2A)}{(6\beta-1)(2\gamma-1)^2} - \frac{\gamma(1-2A\beta)}{5(6\beta-1)(2\gamma-1)^2} + \frac{\gamma(1-2A\beta)\eta}{2(6\beta-1)(2\gamma-1)^2} \right\}. \end{aligned} \quad (45)$$

#### 4. Results and Discussion

In order to verify the accuracy of the homotopy perturbation method, the developed nonlinear equations are also solved using the shooting method coupled with the Runge–Kutta method. Table 4 shows the comparison of the results of the numerical method (NM) and the homotopy perturbation method. From the table, it could be inferred that the results of the present work agree with the results of the numerical method using the shooting method with the Runge–Kutta method.

In order to further establish the accuracy of the solution of the HPM, the results of the present study (in the absence of the slip parameter, i.e., no-slip condition) are further compared with the results of the numerical method using the shooting method with the six-order Runge–Kutta method. The values of the local Nusselt number  $Nu_L$  and local Sherwood number  $Sh_L$  have been calculated for various values of  $Nb$  and  $Nt$ . An excellent agreement found between the two set of results is as shown in Table 5. Therefore, the use of the homotopy perturbation method for the analysis of the double-diffusive models is justified.

In order to further establish the accuracy of the solution of HPM, the results of the present study (in the absence of the slip parameter) are further compared with the results of the numerical method using the shooting method with the Runge–Kutta method as presented in the literature [20]. The values of the local Nusselt number  $Nu_L$  and local Sherwood number  $Sh_L$  have been calculated for various values of  $Nb$  and  $Nt$ . An excellent agreement is found between the two set of results as shown in Table 5. Also, the results that agree with the previous studies using the homotopy analysis method have been presented in the literature [9]. Therefore, the use of the homotopy perturbation method for the analysis of the thermal-diffusion and diffusion-thermal of magnetohydrodynamic squeezing unsteady flow of nanofluid between two parallel disks embedded in a porous medium under the influences of slip and temperature jump conditions is justified.

Figure 2 shows the effects of nanoparticle volume fraction on the nanofluid dynamic viscosity ratio. It is inferred from the results that nanofluid dynamic viscosity ratio decreases as the nanoparticle volume fraction increases. The variation of

nanoparticle volume fraction with thermal conductivities ratio of copper (II) oxide-water nanofluid with different particle shapes is shown in Figure 3. It is depicted in Figure 3 that the thermal conductivity of nanofluid varies linearly and increases with increase in nanoparticle volume fraction. Irrespective of the nanoparticle volume fraction, it is established that the nanofluid with spherical shape nanoparticles has the lowest thermal conductivity ratio while the nanofluid with lamina shape nanoparticles has the highest thermal conductivity ratio. This also shows that the thermal conductivity ratio of the nanofluid is directly proportional to the nanoparticles shape factor. The suspensions of nanoparticles with a high shape factor or low sphericity in a basefluid gives higher thermal conductivity ratio to the fluid as a nanofluid than when nanoparticles with a low shape factor or high sphericity is suspended in the same fluid.

The influence of nanoparticle volume fraction on the velocity of the nanofluid during the squeezing flow is depicted in Figure 4. It is established from the results that as the nanoparticle volume fraction increases, the velocity of the nanofluid increases between  $0 \leq \eta \leq 0.42$  (not accurately determined) because the nanoparticle volume fraction increases the skin friction coefficient of the nanofluid. However, the trend of this effect is reversed when  $\eta > 0.42$ .

Effect of the slip parameter on the velocity profile of the flow process is illustrated in Figure 5. It is shown in the figure that the radial velocity component increases with an increase in the slip parameter near the lower disk, that is,  $\eta > 0$  and  $\eta > 0.5$  (not accurately determined). A reverse case is recorded as the flow approaches the upper disk, that is,  $\eta > 0.5$  and  $\eta < 1$  (not accurately determined). The trend in the graph and the behavior of the fluid as depicted in the figure can be physically explained that as the slip parameter increases, there is a corresponding decrease in shear stress which consequently increases the radial velocity component near the stationary lower disk while a reverse trend occurs as the nanofluid moves and flow approaches the upper disk. Figure 6 shows the effect of the increasing Hartmann parameter ( $M$ ) on the velocity profile of the nanofluid flow between the parallel disk. It is observed as presented in the figure that, at increasing values of  $M$ , the velocity decreases slightly near the lower disk and as the upper disk

TABLE 1: The values of different shapes of nanoparticles [74, 75].

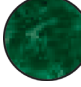



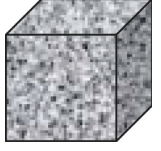
No.	Name	Shape	Shape factor ( $m$ )
1	Spherical		3.0
2	Platelet		5.7
3	Cylinder		4.8
4	Laminar		16.2
5	Brick		3.7

TABLE 2: Physical and thermal properties of the basefluid [74, 75].

Base fluid	$\rho$ (kg/m <sup>3</sup> )	$C_p$ (J/kg K)	$k$ (W/mK)	$\sigma$ ( $\Omega^{-1}\cdot\text{m}^{-1}$ )
Pure water	997.1	4179	0.613	5.50
Ethylene glycol	1115	2430	0.253	1.07
Engine oil	884	1910	0.144	4.02
Kerosene	783	2010	0.145	4.01

TABLE 3: Physical and thermal properties of nanoparticles [74, 75].

Nanoparticles	$\rho$ (kg/m <sup>3</sup> )	$C_p$ (J/kg K)	$k$ (W/mK)	$\sigma$ ( $\Omega^{-1}\cdot\text{m}^{-1}$ )
Copper (Cu)	8933	385	401	59.6
Aluminum oxide (Al <sub>2</sub> O <sub>3</sub> )	3970	765	40	16.7
SWCNTs	2600	42.5	6600	1.26
Silver (Ag)	10500	235.0	429	
Titanium dioxide (TiO <sub>2</sub> )	4250	686.2	8.9538	
Copper (II) oxide (CuO)	783	540	18	

is approached the velocity increases slightly due to the increase in the boundary layer thickness caused by the Lorentz or magnetic force field; that is, for the electrically conducting fluid in the presence of magnetic field, there is a Lorentz force which slows down the motion of the fluid in the boundary layer region. Moreover, during the squeezing flow (when the disks are moving towards each other), the situation together with the Lorentz force creates adverse pressure gradient in the flow. Whenever such forces act over a long time, there might be a point separation and back

TABLE 4: Comparison of values of the temperature jump parameter ( $\gamma$ ) when  $A = 2, S = 1, Nt = Nb = 0.2, \phi = 0, \beta = 0.05, M = 0.5, Le = Pr = 1.0$ , and  $C = 0$ .

$\gamma$	Dimensionless temperature	
	NM	Present work
0.00	1.0000	1.0000
0.10	1.2231	1.2232
0.15	1.4053	1.4053
0.20	1.6214	1.6215
0.25	1.7312	1.7311
0.30	1.8656	1.8656
0.35	2.2013	2.2011
0.40	3.1052	3.1052

TABLE 5: Comparison of the values of the local Nusselt and local Sherwood number for various values of  $Nb$  and  $Nt$  with  $\beta = \phi = \gamma = 0$ .

$Nb$	$Nt$	$Nu_L = -\theta'(1)$			$Sh_L = -\phi'(1)$		
		NM [20]	HAM [9]	Present method	NM [20]	HAM [9]	Present method
0.1	0.1	0.5263	0.5263	0.5263	0.8660	0.8660	0.8660
0.5		0.6343	0.6343	0.6343	0.5301	0.5300	0.5300
1.0		0.7864	0.7864	0.7864	0.4860	0.4860	0.4860
1.5		0.9557	0.9557	0.9556	0.4699	0.4699	0.4698
1.5	0.5	1.1768	1.1768	1.1768	0.4018	0.4018	0.4018
	1.0	1.4858	1.4858	1.4857	0.1262	0.1262	0.1261
	1.5	1.8231	1.8231	1.8230	0.3908	0.3908	0.3908
	2.0	2.1792	2.1792	2.1792	1.1680	1.1678	1.1678

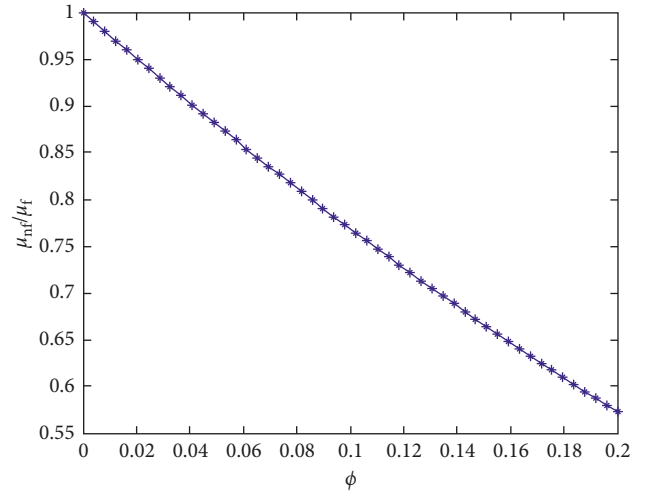


FIGURE 2: Variation of nanofluid dynamic viscosity ratio.

flow occurs. However, when the disks are moving apart, the reason for the behavior is quite different as there exist a vacant space and the nanofluid in that region goes with high velocity so as not to violate the mass conservation. That is, since the mass flow rate is kept conservative, decrease in the fluid velocity near the wall region will be compensated by increasing the fluid velocity near the central region.

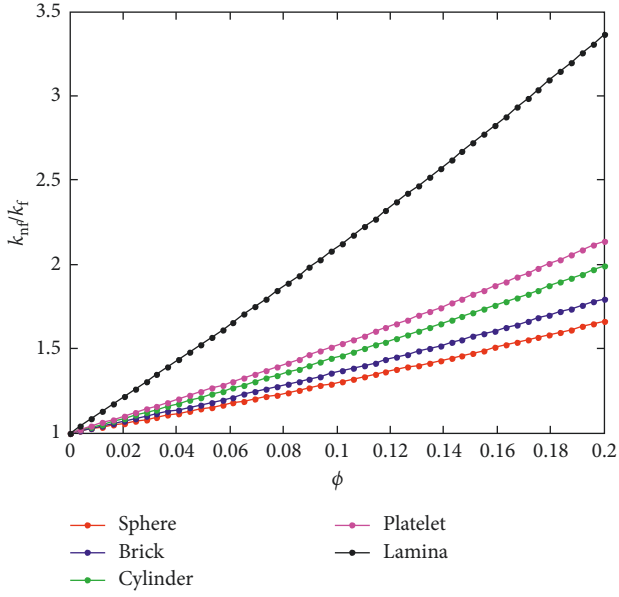


FIGURE 3: Effects of nanoparticle shape on thermal conductivity with nanoparticle volume fraction conductivity ratio of nanofluid.

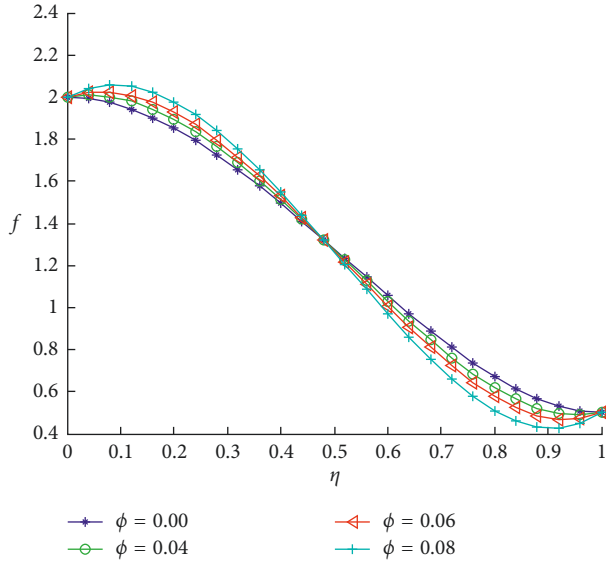


FIGURE 4: Effect of nanoparticle volume fraction on the velocity profile when  $A = 2, S = 1, Nt = Nb = 0.2, \gamma = 0.1, \beta = 0.05, M = 0.5, Le = Pr = 1.0$ , and  $C = -1$ .

As squeeze parameter ( $S$ ) increases which is demonstrated in Figure 7, the radial velocity component increases. The effect is maximum at the lower disk and minimum at the upper disk. Figure 8 depicts the effect of increasing the pressure term ( $C$ ) on the velocity of the fluid flow; it is shown that with, increasing  $C$ , a very slight increase in the velocity component is observed.

The effect of the temperature jump parameter ( $\gamma$ ) on the temperature profile is shown in Figure 9. It is observed that as the temperature jump parameter increases, temperature distribution increases towards the lower disk where

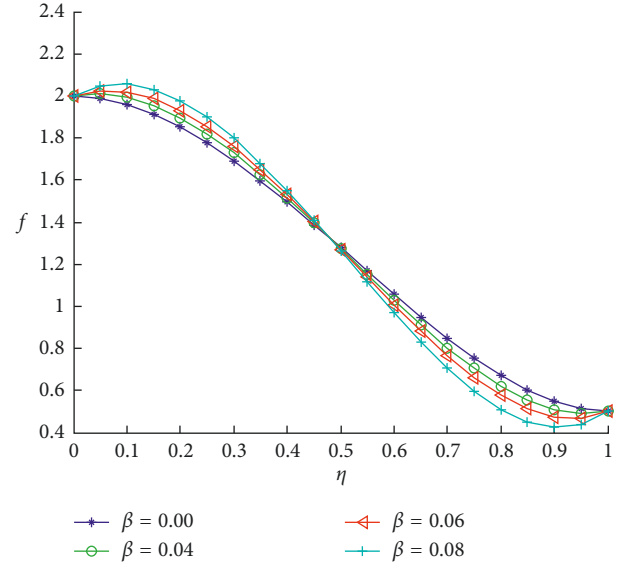


FIGURE 5: Effect of the slip parameter on the velocity profile when  $A = 2, S = 1, Nt = Nb = 0.2, \gamma = 0.1, M = 0.5, Le = Pr = 1.0$ , and  $C = -1$ .

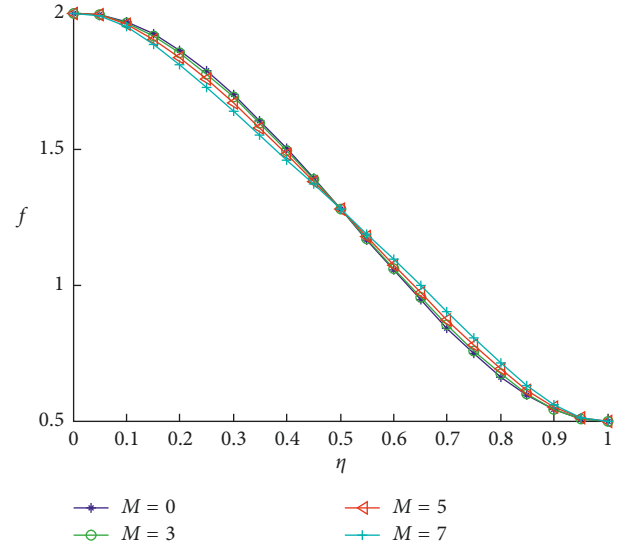


FIGURE 6: Effect of the Hartmann parameter on the velocity profile when  $A = 2, S = 1, Nt = Nb = 0.2, \gamma = 0.1, \beta = 0.05, M = 0.5, Le = Pr = 1.0$ , and  $C = -1$ .

it decreases towards the upper disk. In the absence of slip, that is,  $\gamma = 0$ , it is observed that temperature distribution equals to unity at the lower plate and zero at the upper plate. Influence of the thermophoresis parameter ( $Nt$ ) is demonstrated in Figure 10 which depicts that, with increasing values of  $Nt$ , the temperature distribution increases and is maximum at the lower disk but falls rapidly towards the upper disk. The effect of the squeeze parameter ( $S$ ) on temperature distribution is displayed in Figure 11. The figure illustrates that, at increasing values  $S$ , the temperature distribution at the lower disk reduces while the

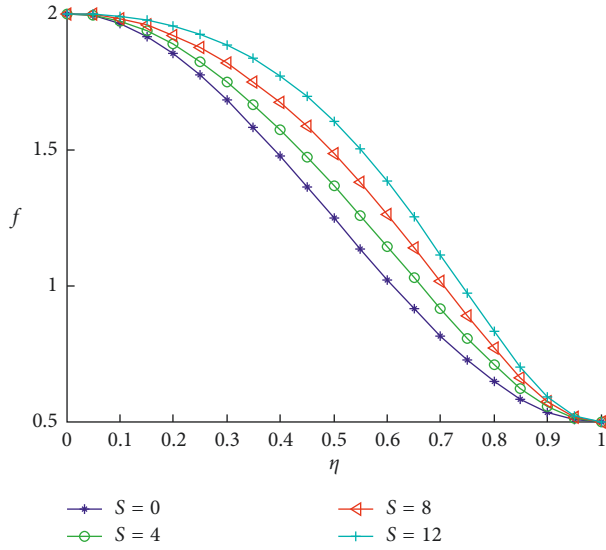


FIGURE 7: Effect of the squeezing parameter on the velocity profile when  $A = 2, S = 1, \beta = 0.05, Nt = Nb = 0.2, \gamma = 0.1, M = 0.5, Le = Pr = 1.0$ , and  $C = -1$ .

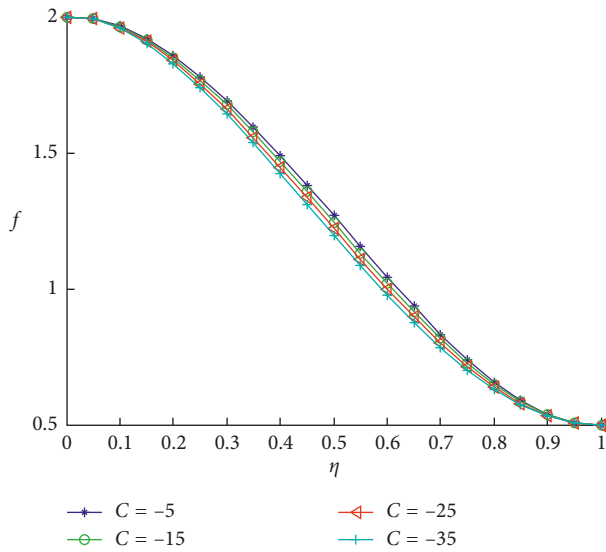


FIGURE 8: Effect of pressure gradient on velocity profile when  $A = 2, S = 1, Nt = Nb = 0.2, \gamma = 0.1, M = 0.5, Le = Pr = 1.0$ , and  $\beta = 0.05$ .

temperature distribution at the upper disk increases which can be physically explained as increase in  $S$  that leads to a corresponding decrease in kinematic viscosity and vice versa. It is obvious from Figure 12 that the increasing pressure term ( $C$ ) has no significant effect on temperature distribution.

Figure 13 displays the influence of nanoparticle volume fraction on the temperature profile of the nanofluid during the squeezing flow. The figure shows that the temperature increases as the nanoparticle volume fraction increases in the nanofluid. The reason behind this behavior is that when the two disks move towards each other (squeezing flow)

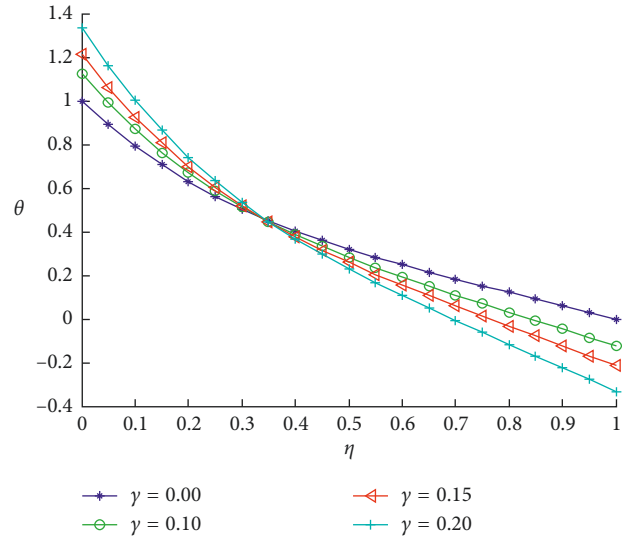


FIGURE 9: Effect of the jump parameter on the temperature profile when  $A = 2, S = 1, Nt = Nb = 0.2, \beta = 0.05, M = 0.5, Le = Pr = 1.0$ , and  $C = -1$ .

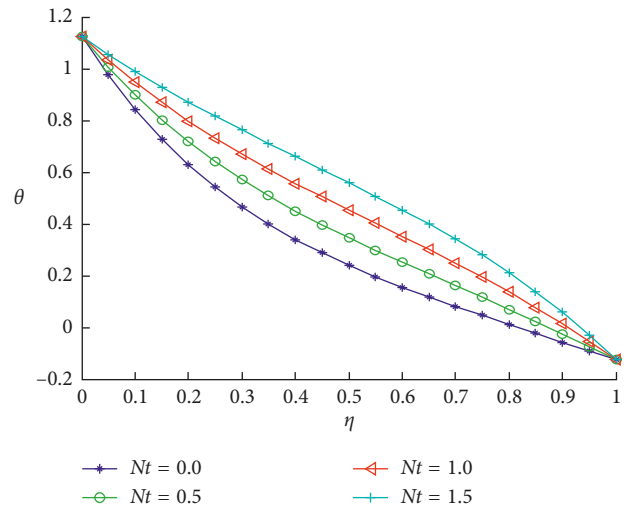


FIGURE 10: Effect of the thermophoresis parameter on the temperature profile when  $A = 2, S = 1, \gamma = 0.1, Nb = 0.2, \beta = 0.05, M = 0.5, Le = Pr = 1.0$ , and  $C = -1$ .

and the nanoparticle volume fraction increases, there is more collision between the nanoparticles and the particles with the boundary surface of the disk. Consequently, the resulting friction gives rise to increases in temperature within the nanofluid near the boundary region. It should be pointed out that an opposite to the trend witnessed during the squeezing flow is established when the disks are moving apart.

The effect of the nanoparticle shape factor on the temperature profile of the nanofluid during the squeezing flow is shown in Figure 14. The different shaped nanoparticles considered are sphere, brick, cylinder, and lamina. It is shown from the figure that the temperature increases

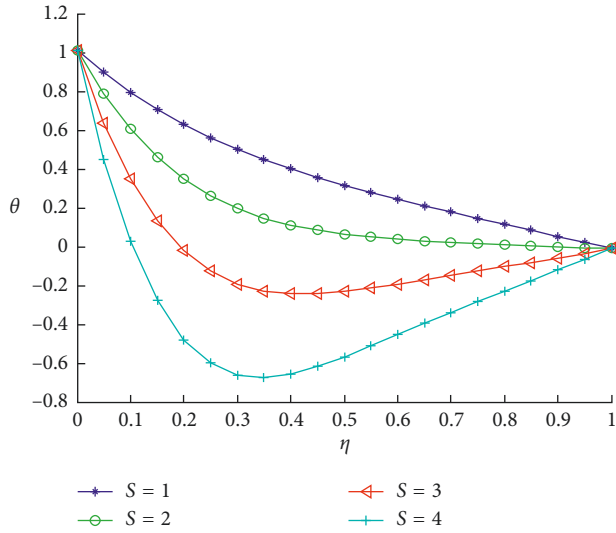


FIGURE 11: Effect of the squeeze parameter on the temperature profile when  $A = 2$ ,  $\gamma = 0.1$ ,  $Nt = Nb = 0.2$ ,  $\beta = 0.05$ ,  $M = 0.5$ ,  $Le = Pr = 1.0$ , and  $C = 1$ .

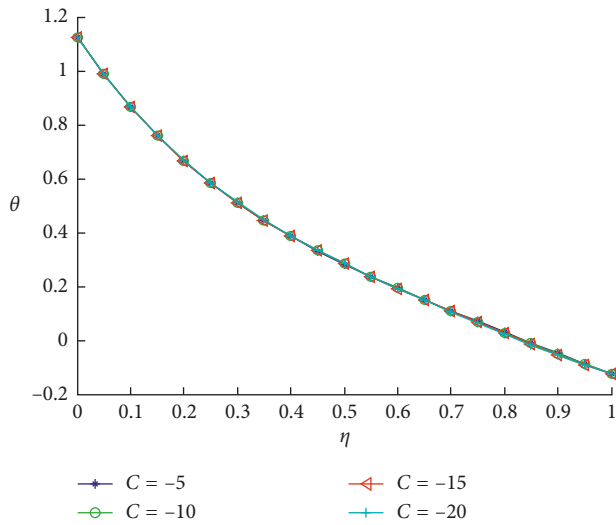


FIGURE 12: Effect of the pressure gradient on the temperature profile when  $A = 2$ ,  $S = 1$ ,  $Nt = Nb = 0.2$ ,  $\beta = 0.05$ ,  $M = 0.5$ ,  $Le = Pr = 1.0$ , and  $\gamma = 0.1$ .

as the nanoparticle shape factor increases. This is because thermal conductivity of the nanofluid increases with increase in the nanoparticle shape factor. Regardless of the nanoparticle volume fraction, it is established that the nanofluid with spherical shape nanoparticles has the lowest thermal conductivity ratio while the nanofluid with lamina shape nanoparticles has the highest thermal conductivity ratio. The suspensions of nanoparticles with a high shape factor or low sphericity in a basefluid gives higher thermal conductivity ratio to the fluid as a nanofluid than when nanoparticles with a low shape factor or high sphericity is suspended in the same fluid. Therefore, as the nanoparticle volume fraction increases due to the

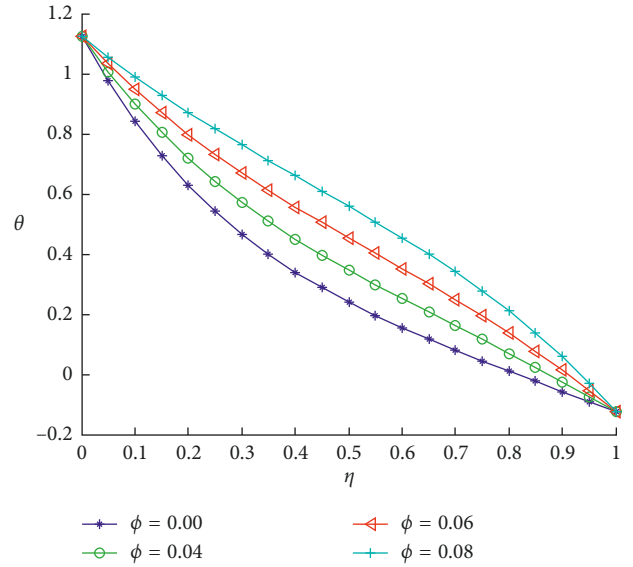


FIGURE 13: Effect of nanoparticle volume fraction on the temperature profile when  $A = 2$ ,  $S = 1$ ,  $Nt = Nb = 0.2$ ,  $\beta = 0.05$ ,  $M = 0.5$ ,  $Le = Pr = 1.0$ ,  $\gamma = 0.1$ , and  $C = -1$ .

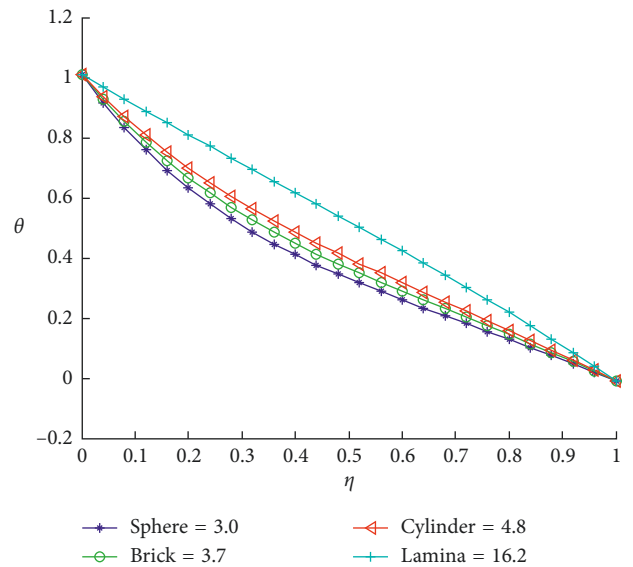


FIGURE 14: Effect of the nanoparticle shape factor on the temperature profile when  $A = 2$ ,  $S = 1$ ,  $Nt = Nb = 0.2$ ,  $\beta = 0.05$ ,  $M = 0.5$ ,  $Le = Pr = 3.0$ ,  $\gamma = 0.1$ , and  $C = -1$ .

increased shape factor, there are increased interactions and collisions between the nanoparticles and the particles with the boundary surface of the disk, and as a consequence, more friction is created that gives rise to increase in temperature within the nanofluid near the boundary region.

Influence of the Lewis number ( $Le$ ) on the concentration profile of the nanofluid flow process is depicted in Figure 15. It is illustrated that increasing  $Le$  evokes a corresponding increase in concentration distribution at the

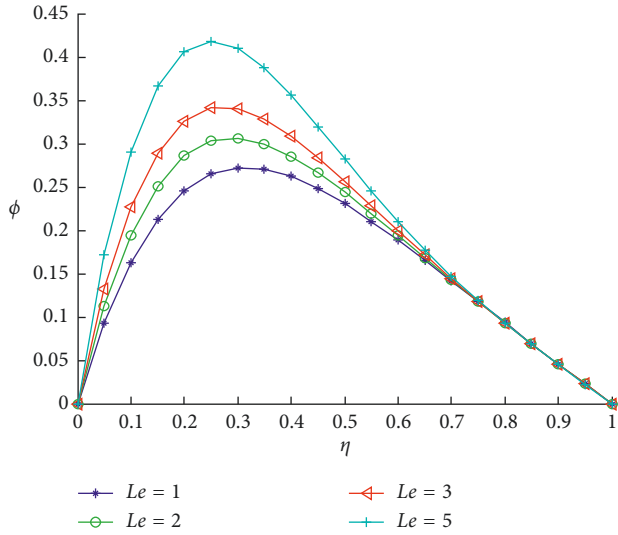


FIGURE 15: Effect of the Lewis number on the concentration profile when  $A = 2, S = 1, Nt = Nb = 0.2, \beta = 0.05, M = 0.5, \gamma = 0.1, Pr = 1.0$ , and  $C = -1$ .

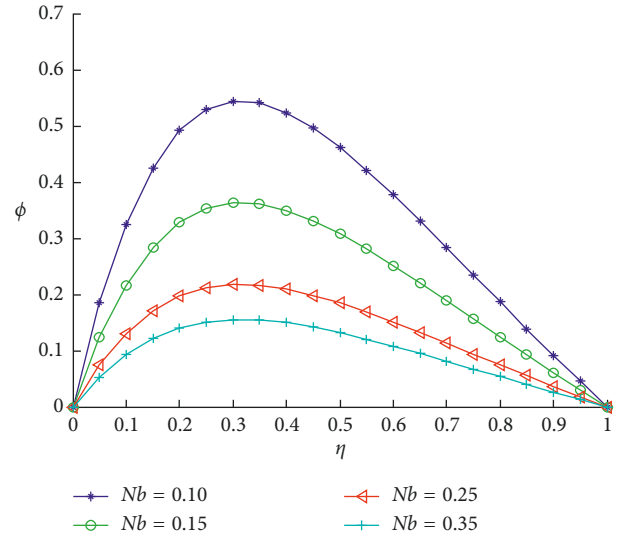


FIGURE 17: Effect of the Brownian motion parameter on the concentration profile when  $A = 2, S = 1, Nt = 0.2, \gamma = 0.1, \beta = 0.05, M = 0.5, Le = Pr = 1.0$ , and  $C = -1$ .

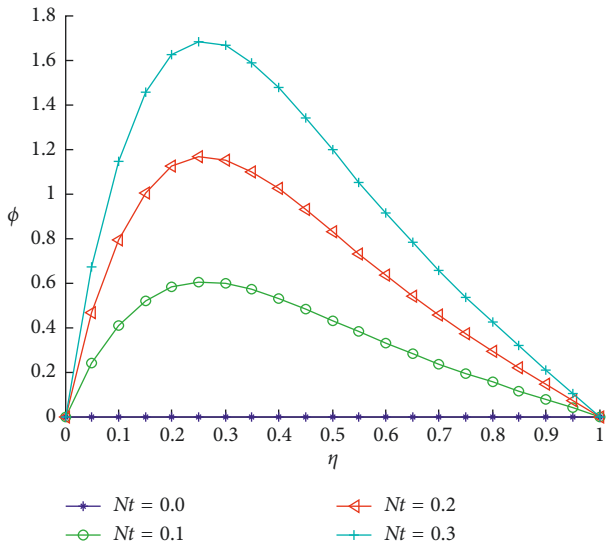


FIGURE 16: Effect of the thermophoresis parameter on the concentration profile when  $A = 2, S = 1, \gamma = 0.1, Nb = 0.2, \beta = 0.05, M = 0.5, Le = Pr = 1.0$ , and  $C = -1$ .

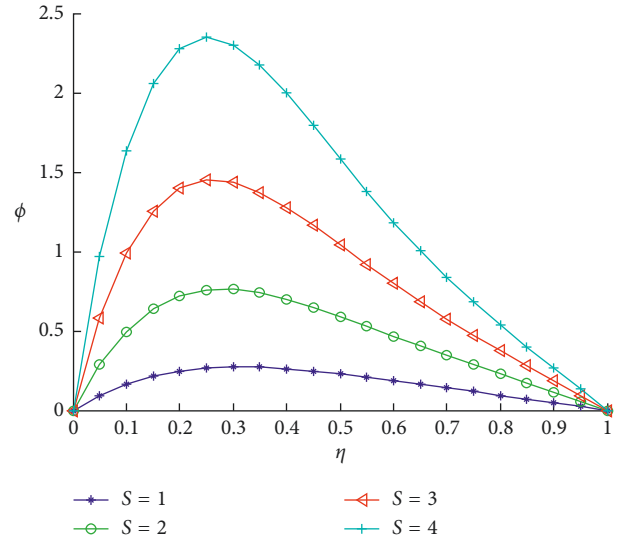


FIGURE 18: Effect of the squeeze parameter on the concentration profile when  $A = 2, Nt = Nb = 0.2, \gamma = 0.1, \beta = 0.05, M = 0.5, Le = Pr = 1.0$ , and  $C = -1$ .

region closer to the lower disk, though it decreases rapidly as it moves towards the upper disk. Thermophoresis parameter ( $Nt$ ) effect on the concentration profile of the flow of nanofluid is observed in Figure 16, at increasing values of  $Nt$  the concentration profile increases significantly but towards the upper disk there is a steady reduction. Figure 17 depicts the effect of the Brownian motion parameter ( $Nb$ ) on the concentration profile of the nanofluid flow. As observed and presented in the figure, it is established that increasing value of  $Nb$  concentration profile decreases significantly, which falls rapidly as it approaches the upper disk at suction. Also, when the squeeze parameter ( $S$ ) is

increased, the effect on the concentration profile of the nanofluid flow process is shown in Figure 18. From the figure, it is shown that the concentration distribution increases significantly near the wall close to the lower disk but falls rapidly as the upper disk is approached during suction. Figures 19 and 20 display the influence of nanoparticle volume fraction and nanoparticle shape factor on the concentration profile of the nanofluid, respectively. It can be seen in the figure that a maximum temperature occurs between  $0.2 < \eta < 0.3$  for all the nanoparticle volume fraction and nanoparticle shape factor considered. The figure shows that the concentration



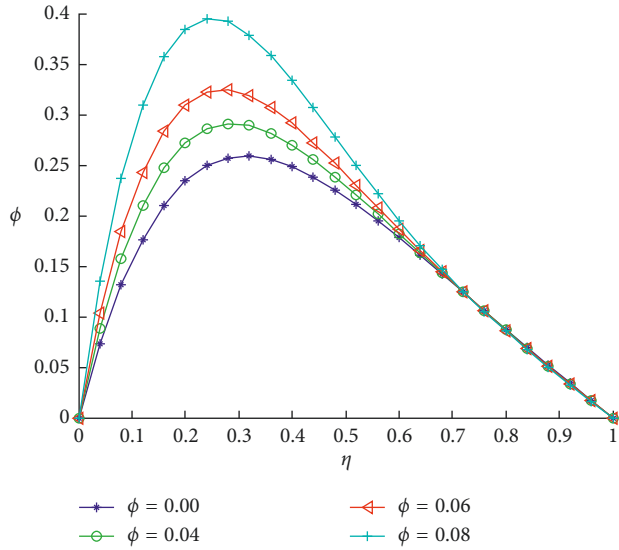


FIGURE 19: Effect of nanoparticle volume fraction on the concentration profile when  $A = 2$ ,  $S = 1$ ,  $Nt = Nb = 0.2$ ,  $\beta = 0.05$ ,  $M = 0.5$ ,  $Le = Pr = 1.0$ ,  $\gamma = 0.1$ , and  $C = -1$ .

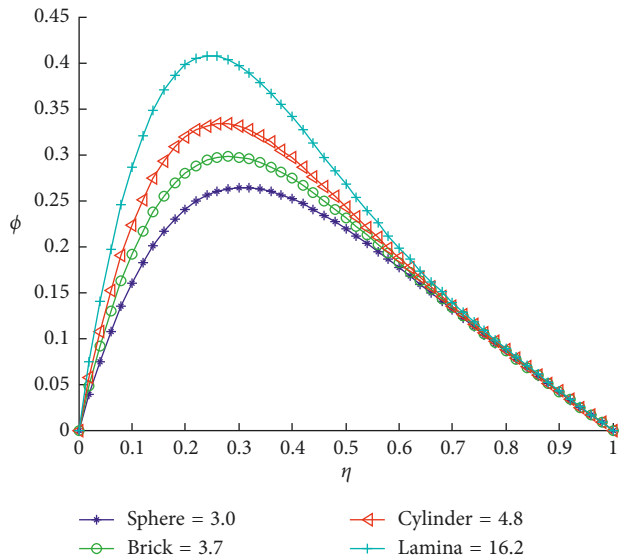


FIGURE 20: Effect of the nanoparticle shape factor on the concentration profile when  $A = 2$ ,  $S = 1$ ,  $Nt = Nb = 0.2$ ,  $\beta = 0.05$ ,  $M = 0.5$ ,  $Le = Pr = 1.0$ ,  $\gamma = 0.1$ , and  $C = -1$ .

of the nanofluid increases as the nanoparticle volume fraction and nanoparticle shape factor increase. The increase of nanoparticle volume fraction or the use of nanoparticle with a high shape factor in a basefluid increases the surface area for chemical reaction. Therefore, as the nanoparticle volume fraction or nanoparticle shape factor increases, there are increased chemical interactions between the nanoparticles and the particles with the boundary surface of the disk, and as a consequence, more species are formed which increase the concentration of the species within the nanofluid.

## 5. Conclusion

In this study, effects of nanoparticle geometry, slip, and temperature jump conditions on thermo-magneto-solutal squeezing flow of nanofluid between two parallel disks embedded in a porous medium have been investigated analytically using the homotopy perturbation method. Also, the influences of various flow parameters such as thermophoresis, the Brownian motion, and the Lewis number and pressure gradient on flow, heat, and mass transfer of the process were investigated. It is established in the study that the addition of nanoparticles to the basefluid enhances its thermal conductivity. Based on the study, the following remarks were made:

- (i) Irrespective of the nanoparticle volume fraction, the thermal conductivity ratio of the nanofluid is directly proportional to the nanoparticles shape factor. This fact presents overall effects on the velocity, temperature, and concentration of the nanofluid during the flow process.
- (ii) The radial velocity component increases with an increase in the slip parameter near the lower disk. A reverse case is recorded as the flow approaches the upper disk.
- (iii) Increasing the values of the magnetic field parameter, the velocity decreases slightly near the lower disk and increases towards the upper disk.
- (iv) As the squeeze number increases, the radial velocity component increases and the temperature distribution at the lower disk decreases, while the temperature at the upper disk increases and the concentration distribution increases significantly near the wall close to the lower disk but falls rapidly as the upper disk is approached during suction.
- (v) Increasing the pressure gradient term, a very slight increase in the velocity component was observed while the pressure gradient term has no significant effect on temperature distribution.
- (vi) The temperature and concentration of the nanofluid increase as the nanoparticle volume fraction and nanoparticle shape factor of the nanofluid increase.
- (vii) As the temperature jump parameter increases, temperature distribution increases towards the lower disk where it decreases towards the upper disk.
- (viii) Increasing values of the thermophoresis parameter, the temperature distribution increases and is maximum at the lower disk but falls rapidly towards the upper disk, while the concentration profile increases significantly, but towards the upper disk there is a steady reduction.
- (ix) Also, increasing the Lewis number evokes a corresponding increase in concentration distribution at the region closer to the lower disk.



- (x) Increasing the value of the Brownian number, the concentration profile decreases significantly, which falls rapidly as it approaches the upper disk at suction.

Important significance of the study includes energy conservation, friction reduction, and micromixing of biological samples.

## Nomenclature

$A$ :	Suction/injection parameter
$B$ :	Magnetic field strength (Nm/A)
$c$ :	Concentration ( $\text{kg/m}^3$ )
$C$ :	Pressure gradient term
$c_p$ :	Specific heat capacity at constant pressure (J/kg K)
$c_w$ :	Specific heat capacity of the nanofluid (J/kg K)
$D_B$ :	Brownian motion coefficient ( $\text{m}^2/\text{s}$ )
$D_T$ :	Thermophoretic diffusion coefficient ( $\text{m}^2/\text{s}$ )
$h$ :	Height of the flow (m)
$H$ :	Total distance between the two disks (m)
$k_{nf}$ :	Thermal conductivity of the nanofluid (W/mK)
$K_p$ :	Permeability of the porous medium ( $\text{m}^2$ )
$Le$ :	Lewis number
$M$ :	Hartmann number or magnetic field parameter
$Nt$ :	Thermophoresis parameter
$Nb$ :	Brownian motion parameter
$P$ :	Pressure ( $\text{N/m}^2$ )
$Pr$ :	Prandtl's number
$r$ :	Radius of the disk (m)
$S$ :	Squeeze number
$t$ :	Time (s)
$T$ :	Temperature (K)
$\mu_f$ :	Dynamic viscosity of the basefluid (Ns/ $\text{m}^2$ )
$\mu_{nf}$ :	Dynamic viscosity of the nanofluid (Ns/ $\text{m}^2$ )
$\rho_{nf}$ :	Nanofluid density ( $\text{kg/m}^3$ )
$\alpha_{nf}$ :	Thermal diffusivity of the nanofluid ( $\text{m}^2/\text{s}$ )
$(\rho C_p)_{nf}$ :	Heat capacity of the nanofluid ( $\text{Jm}^3/\text{K}$ )
$\rho_f$ :	Density of the basefluid ( $\text{kg/m}^3$ )
$\phi$ :	Dimensionless nanoconcentration parameter
$\theta$ :	Dimensionless temperature
$w$ :	Axial velocity component (m/s)
$u$ :	Radial velocity component (m/s)
$\eta$ :	Similarity variable
$\beta$ :	Dimensionless slip velocity parameter
$\gamma$ :	Dimensionless temperature jump parameter
$\tau$ :	Ratio of nanoparticle heat capacity to basefluid
$\sigma$ :	Electrical conductivity ( $\Omega\text{m}$ )
$\nu$ :	Kinematic viscosity ( $\text{m}^2/\text{s}$ )
$\alpha$ :	Thermal diffusivity ( $\text{m}^2/\text{s}$ ).

## Conflicts of Interest

The authors declare that there are no conflicts of interest regarding the publication of this paper.

## References

- [1] M. Mustafa, T. Hayat, and S. Obadiat, "On heat and mass transfer in the unsteady squeezing flow between parallel plates," *Mechanica*, vol. 47, no. 7, pp. 1581–1589, 2012.
- [2] T. Hayat, A. Yousaf, M. Mustafa, and S. Obadiat, "MHD squeezing flow of second grade fluid between two parallel disk," *International Journal of Numerical Fluids*, vol. 69, no. 2, pp. 399–410, 2011.
- [3] G. Domairry and A. Aziz, "Approximate analysis of MHD squeeze flow between two parallel disks with suction or injection by homotopy perturbation method," *Mathematical Problems in Engineering*, vol. 2009, article 603916, 19 pages, 2009.
- [4] A. M. Siddiqui, S. Irum, and A. R. Ansari, "Unsteady squeezing flow of a viscous MHD fluid between parallel plates," *Mathematical Modeling and Analysis*, vol. 13, no. 4, pp. 565–576, 2008.
- [5] A. M. Rashidi, H. Shahmohamadi, and S. Dinarvand, "Analytic approximate solutions for unsteady two dimensional and axisymmetric squeezing flows between parallel plates," *Mathematical Problems in Engineering*, vol. 2008, article 935095, 12 pages, 2008.
- [6] W. A. Khan and A. Aziz, "Natural convective boundary layer flow over a vertical plate with uniform surface heat flux," *International Journal of Thermal Sciences*, vol. 50, no. 7, pp. 1207–1217, 2011.
- [7] W. A. Khan and A. Aziz, "Double diffusive natural convection boundary layer flow in a porous medium saturated with a nanofluid over a vertical plate, prescribed surface heat, solute and nanofluid fluxes," *International Journal of Thermal Sciences*, vol. 50, no. 11, pp. 2154–2160, 2011.
- [8] A. J. Kuznetsov and N. D. Nield, "Natural convective boundary layer flow of a nanofluid past a vertical plate," *International Journal of Thermal Sciences*, vol. 49, no. 2, pp. 243–247, 2010.
- [9] M. R. Hashimi, T. Hayat, and A. Alsaedi, "On the analytic solutions for squeezing flow of nanofluids between parallel disks," *Nonlinear Analysis Modeling and Control*, vol. 17, no. 4, pp. 418–430, 2014.
- [10] C. H. Choi, J. A. Westin, and K. S. Breur, "To slip or not slip water flows in hydrophilic and hydrophobic microchannels," in *Proceedings of IMECE 2002*, New Orleans, LA, USA, November 2002.
- [11] M. T. Matthew and I. D. Boyd, "Nano boundary layer equation with nonlinear Navier boundary condition," *Journal of Mathematical Analysis and Application*, vol. 333, no. 1, pp. 381–400, 2007.
- [12] M. J. Martin and L. D. Boyd, "Momentum and heat transfer in a laminar boundary layer with slip flow," *Journal of Thermo Physics and Heat Transfer*, vol. 20, no. 4, pp. 710–719, 2006.
- [13] P. D. Ariel, "Axisymmetric flow due to stretching sheet with partial slip," *Computer and Mathematics with Application*, vol. 333, pp. 381–400, 2007.
- [14] C. Wang, "Analysis of viscous flow due to a stretching sheet with surface slip and suction," *Nonlinear Analysis: Real World Application*, vol. 10, no. 1, pp. 375–380, 2009.
- [15] K. Das, "Impact of thermal radiation on MHD slip flow over a flat plate with variable fluid properties," *Heat and Mass Transfer*, vol. 48, no. 5, pp. 767–778, 2012.
- [16] K. Das, "Slip effects on heat and mass transfer in MHD micro polar fluid flow over an inclined plate with thermal radiation and chemical reaction," *International Journal of Numerical Methods in Fluids*, vol. 70, no. 1, pp. 96–101, 2016.
- [17] A. Hussain, S. T. Mohyud-Cheema, and T. A. Din, "Analytical and numerical approaches to squeezing flow and heat transfer between two parallel disks with velocity slip and temperature jump," *China Physics Letter*, vol. 29, no. 11, pp. 1–5, 2012.

- [18] K. Das, "Slip flow and convective heat transfer of nanofluid over a permeable stretching surface," *Computers and Physics*, vol. 64, no. 1, pp. 34–42, 2012.
- [19] R. G. Deissler, "An analysis of second-order slip flow and temperature-jump boundary conditions for rarefied gases," *International Journal of Heat and Mass Transfer*, vol. 7, no. 6, pp. 681–694, 1964.
- [20] K. Das, S. Jana, and N. Acharya, "Slip effects on squeezing flow of nanofluid between two parallel disks," *International Journal of Applied Mechanics and Engineering*, vol. 21, no. 1, pp. 5–20, 2016.
- [21] R. Ellahi, T. Hayat, F. M. Mahomed, and S. Asghar, "Effects of slip on nonlinear flows of a third grade fluid," *Nonlinear Analysis: Real World Applications*, vol. 11, no. 1, pp. 139–146, 2010.
- [22] C. L. M. H. Navier, "Memoir sur les lois du mouvement des fluids," *Memoirs Academic Royal Science Institute France*, vol. 6, pp. 389–440, 1823.
- [23] S. Yao, T. Fang, and Y. Zhang, "Heat transfer of a generalized stretching/shrinking wall problem with convective boundary condition," *Communications in Nonlinear Science and Numerical Simulation*, vol. 16, no. 2, pp. 752–760, 2011.
- [24] R. Kandasamy, P. Loganathanb, and P. P. Arasub, "Scaling group transformation for MHD boundary layer flow of a nanofluid past vertical stretching surface in the presence of suction/injection," *Nuclear Engineering and Design*, vol. 241, no. 6, pp. 2053–2059, 2011.
- [25] D. Makinde and A. Aziz, "Boundary layer flow of a nanofluid past a stretching sheet with convective boundary conditions," *International Journal of Thermal Sciences*, vol. 50, no. 7, pp. 1326–1332, 2011.
- [26] M. J. Uddin, Y. Alginahi, O. Anwar Bég, and M. N. Kabir, "Numerical solutions for gyrotactic bioconvection in nanofluid-saturated porous media with Stefan blowing and multiple slip effects," *Computers and Mathematics with Applications*, vol. 72, no. 10, pp. 2562–2581, 2016.
- [27] M. J. Uddin, M. N. Kabir, and Y. M. Alginahi, "Lie group analysis and numerical solution of magnetohydrodynamic free convective slip flow of micropolar fluid over a moving plate with heat transfer," *Computers and Mathematics with Applications*, vol. 70, no. 5, pp. 846–856, 2015.
- [28] J. Uddin, W. A. Khan, and A. I. Ismail, "Scaling group transformation for MHD boundary layer slip flow of a nanofluid over a convectively heated stretching sheet with heat generation," *Mathematical Problems in Engineering*, vol. 2012, article 934964, 20 pages, 2012.
- [29] J. Uddin, O. Anwar Bég, and A. I. Ismail, "Radiative convective nanofluid flow past a stretching/shrinking sheet with slip effects," *Journal of Thermophysics and Heat Transfer*, vol. 29, no. 3, pp. 513–523, 2015.
- [30] J. Uddin, O. A. Bég, A. Aziz, and A. I. Ismail, "Group analysis of free convection flow of a magnetic nanofluid with chemical reaction," *Mathematical Problems in Engineering*, vol. 2015, article 621503, 11 pages, 2015.
- [31] J. Uddin, O. Anwar Bég, and N. Uddin, "Energy conversion under conjugate conduction, magneto-convection, diffusion and nonlinear radiation over a non-linearly stretching sheet with slip and multiple convective boundary conditions," *Energy*, vol. 115, pp. 1119–1129, 2016.
- [32] T. Zohra, T. Fatema, M. Jashim Uddin, M. Ismail, A. Izani, and O. Anwar Bég, "Bioconvective electromagnetic nanofluid transport from a wedge geometry: simulation of smart electro-conductive bio-nanopolymer processing," *Heat Transfer—Asian Research*, vol. 47, no. 1, pp. 231–250, 2017.
- [33] F. T. Zohra, M. J. Uddin, A. I. M. Ismail, O. A. Bég, and A. Kadir, "Anisotropic slip magneto-bioconvection flow from a rotating cone to a nanofluid with Stefan blowing effects," *Chinese Journal of Physics*, vol. 56, no. 1, pp. 432–448, 2017.
- [34] M. J. Uddin, W. A. Khan, F. T. Zohra, and A. I. M. Ismail, "Blasius and Sakiadis slip flows of nanofluid with radiation effects," *Journal of Aerospace Engineering*, vol. 29, no. 4, p. 04015080, 2016.
- [35] K. V. S. Raju, T. Sudhakar Reddy, M. C. Raju, P. V. Satya Narayana, and S. Venkataramana, "MHD convective flow through porous medium in a horizontal channel with insulated and impermeable bottom wall in the presence of viscous dissipation and Joule heating," *Ain Shams Engineering Journal*, vol. 5, no. 2, pp. 543–551, 2014.
- [36] L. Bühler, C. Mistrangelo, and T. Najuch, "Magnetohydrodynamic flows in model porous structures," *Fusion Engineering and Design*, vol. 98–99, pp. 1239–1243, 2015.
- [37] C. Geindreau and J. L. Auriault, "Magnetohydrodynamic flow through porous media. Ecoulement magnétohydrodynamique en milieux poreux," *Comptes Rendus de l'Académie des Sciences-Series IIB-Mechanics*, vol. 329, no. 6, pp. 445–450, 2001.
- [38] J. A. Falade, J. C. Ukaegbu, A. C. Egere, and S. O. Adesanya, "MHD oscillatory flow through a porous channel saturated with porous medium," *Alexandria Engineering Journal*, vol. 56, no. 1, pp. 147–152, 2017.
- [39] J. R. Pattnaik, G. C. Dash, and S. Singh, "Radiation and mass transfer effects on MHD flow through porous medium past an exponentially accelerated inclined plate with variable temperature," *Ain Shams Engineering Journal*, vol. 8, no. 1, pp. 67–75, 2017.
- [40] F. Ali, I. Khan, S. U. Haq, and S. Shafie, "Influence of thermal radiation on unsteady free convection MHD flow of Brinkman type fluid in a porous medium with Newtonian heating," *Mathematical Problems in Engineering*, vol. 2013, article 632394, 13 pages, 2013.
- [41] A. Khan, I. Khan, F. Ali, and S. Shafie, "Effects of wall shear stress on MHD conjugate flow over an inclined plate in a porous medium with ramped wall temperature," *Mathematical Problems in Engineering*, vol. 2014, article 861708, 15 pages, 2014.
- [42] Z. Ismail, I. Khan, N. M. Nasir, R. Jusoh Awang, M. Z. Salleh, and S. Shafie, "The effects of magnetohydrodynamic and radiation on flow of second grade fluid past an infinite inclined plate in porous medium," *Proceedings of AIP Conference*, vol. 1643, p. 563, 2015.
- [43] Z. Ismail, I. Khan, A. Q. Mohamad, and S. Shafie, "Second grade fluid for rotating MHD of an unsteady free convection flow in a porous medium," *Defect Diffusion Forum*, vol. 362, pp. 100–107, 2015.
- [44] Z. Ismail, I. Khan, and S. Shafie, "Rotation and heat absorption effects on unsteady MHD free convection flow in a porous medium past an infinite inclined plate with ramped wall temperature, Recent Advances in Mathematics," in *Proceedings of 1st International Conference on Mathematical, Computational and Statistical Sciences*, pp. 161–167, 2013.
- [45] M. Hatami, J. Hatami, and D. D. Ganji, "Computer simulation of MHD blood conveying gold nanoparticles as a third grade non-Newtonian nanofluid in a hollow porous vessels," *Computer Method and Program in Biomedicine*, vol. 113, no. 2, pp. 632–641, 2014.
- [46] A. Malvandi and D. D. Ganji, "Magnetic field effect on nanoparticles migration and heat transfer of water/alumina nanofluid in a channel," *Journal of Magnetism and Magnetic Materials*, vol. 362, pp. 172–179, 2014.

- [47] M. Sheikholeslami, M. Hatami, and D. D. Ganji, "Analytical investigation of MHD nanofluid flow in a semi-porous channel," *Powder Technology*, vol. 246, pp. 327–336, 2013.
- [48] M. Fakour, A. Vahabzadeh, D. D. Ganji, and M. Hatami, "Analytical study of micropolar fluid flow and heat transfer in a channel with permeable walls," *Journal of Molecular Liquids*, vol. 204, pp. 198–204, 2015.
- [49] M. Jashim, O. Uddin, A. Beg, and A. I. Ismail, "Mathematical modeling of radiative hydromagnetic thermosolute nanofluid convection slip flow in saturated porous media," *Mathematical Problems in Engineering*, vol. 2014, article 179172, 11 pages, 2014.
- [50] T. Hayat, M. U. Qureshi, and Q. Hussain, "Effect of heat transfer on the peristaltic flow of an electrically conducting fluid in a porous space," *Applied Mathematical Modelling*, vol. 33, no. 4, pp. 1862–1873, 2009.
- [51] M. Hatami, R. Nouri, and D. D. Ganji, "Forced convection analysis for MHD  $\text{Al}_2\text{O}_3$ -water nanofluid flow over a horizontal plate," *Journal of Molecular Liquids*, vol. 187, pp. 294–301, 2013.
- [52] M. Hatami and D. D. Ganji, "Heat transfer and nanofluid flow in suction and blowing process between parallel disks in presence of variable magnetic field," *Journal of Molecular Liquids*, vol. 190, pp. 159–168, 2013.
- [53] M. Sheikholeslami, M. Gorji-Bandpy, R. Ellahi, M. Hassan, and S. Soleimani, "Effects of MHD on Cu water nano fluid flow and heat transfer by means of CVFEM," *Journal of Magnetism and Magnetic Materials*, vol. 349, pp. 188–200, 2014.
- [54] M. Sheikholeslami, M. Gorji-Bandpy, and D. D. Ganji, "Magnetic field effects on natural convection around a horizontal circular cylinder inside a square enclosure filled with nanofluid," *International Communications in Heat and Mass Transfer*, vol. 39, no. 7, pp. 978–986, 2012.
- [55] M. Sheikholeslami, M. Gorji-Bandpy, D. D. Ganji, and S. Soleimani, "Heat flux boundary condition for nanofluid filled enclosure in presence of magnetic field," *Journal of Molecular Liquids*, vol. 193, pp. 174–184, 2014.
- [56] M. Sheikholeslami, M. Gorji-Bandpy, D. D. Ganji, and S. Soleimani, "Effect of a magnetic field on natural convection in an enclosure between a circular and sinusoidal cylinder in the presence of magnetic field," *International Communications in Heat and Mass Transfer*, vol. 39, no. 9, pp. 1435–1443, 2012.
- [57] M. Sheikholeslami and M. Gorji-Bandpy, "Free convection of ferrofluid in a cavity heated from below in the presence of an external magnetic field," *Powder Technology*, vol. 256, pp. 490–498, 2014.
- [58] M. Sheikholeslami, K. Vajravelu, and M. M. Rashidi, "Forced convection heat transfer in a semi annulus under the influence of a variable magnetic field," *International Journal of Heat and Mass Transfer*, vol. 92, pp. 339–348, 2016.
- [59] M. Sheikholeslami, M. Gorji-Bandpy, D. D. Ganji, P. Rana, and S. Soleimani, "Magnetohydrodynamics free convection of  $\text{Al}_2\text{O}_3$ -water nanofluid considering thermophoresis and Brownian motion effects," *Computers and Fluids*, vol. 94, pp. 147–160, 2014.
- [60] M. Sheikholeslami, D. D. Ganji, M. Y. Javed, and R. Ellahi, "Effect of thermal radiation on magnetohydrodynamics nanofluid flow and heat transfer by means of two phase model," *Journal of Magnetism and Magnetic Materials*, vol. 374, pp. 36–43, 2015.
- [61] T. Hayat, T. Muhammad, A. Alsaedi, and M. S. Alhuthali, "Magnetohydrodynamics three-dimensional flow of visco-elastic nanofluid in the presence of nonlinear thermal radiation," *Journal of Magnetism and Magnetic Materials*, vol. 385, pp. 222–229, 2015.
- [62] T. Hayat, M. Rashid, M. Imtiaz, and A. Alsaedi, "Magneto-hydrodynamics (MHD) flow of Cu-water nanofluid due to a rotating disk with partial slip," *AIP Advances*, vol. 5, no. 6, p. 067169, 2015.
- [63] T. Hayat, F. M. Abbasi, M. Al-Yami, and S. Monaqueel, "Slip and Joule heating effects in mixed convection peristaltic transport of nanofluid with Soret and Dufour effects," *Journal of Molecular Liquids*, vol. 194, pp. 93–99, 2014.
- [64] M. M. Rashidi, N. Vishnu Ganesh, A. K. Abdul Hakeem, and B. Ganga, "Buoyancy effect on MHD flow of nanofluid over a stretching sheet in the presence of thermal radiation," *Journal of Molecular Liquids*, vol. 198, pp. 234–238, 2014.
- [65] Z. Mehrez, A. ElCafsi, A. Belghith, and P. LeQuérés, "MHD effects on heat transfer and entropy generation of nanofluid flow in an open cavity," *Journal of Magnetism and Magnetic Materials*, vol. 374, pp. 214–224, 2015.
- [66] F. Mabood, W. A. Khan, and A. I. M. Ismail, "MHD boundary layer flow and heat transfer of nanofluids over a nonlinear stretching sheet: a numerical study," *Journal of Magnetism and Magnetic Materials*, vol. 374, pp. 569–576, 2015.
- [67] F. M. Abbasi, S. A. Shehzad, T. Hayyat, A. Alsadi, and M. A. Obid, "Influence of heat and mass flux conditions in hydromagnetic flow of Jeffrey nanofluid," *AIP Advances*, vol. 5, no. 3, p. 037111, 2015.
- [68] S. A. Shehzad, F. M. Abbasi, T. Hayyat, and A. Alsadi, "MHD mixed convective peristaltic motion of nanofluid with joule heating and thermophoresis effects," *PLoS One*, vol. 9, no. 11, article e111417, 2014.
- [69] J. H. He, "Homotopy perturbation technique," *Computer Methods in Applied Mechanics and Engineering*, vol. 178, no. 3–4, pp. 257–262, 1999.
- [70] J. H. He, "New interpretation of homotopy perturbation method," *International Journal of Modern Physics B*, vol. 20, pp. 2561–2568, 2006.
- [71] J. H. He, "A coupling method of homotopy technique and perturbation technique for nonlinear problems," *International Journal of Non-Linear Mechanics*, vol. 35, pp. 37–43, 2000.
- [72] J. H. He, "Some asymptotic methods for strongly nonlinear equations," *International Journal of Modern Physics B*, vol. 20, pp. 1141–1199, 2006.
- [73] J. H. He, "New perturbation technique which is also valid for large parameters," *Journal of Sound and Vibration*, vol. 229, pp. 1257–1263, 2000.
- [74] R. Kandasamy, R. Mohammad, N. A. B. M. Zailani, and N. F. B. Jaafar, "Nanoparticle shapes on squeezed MHD nanofluid flow over a porous sensor surface," *Journal of Molecular Liquids*, vol. 233, pp. 156–165, 2017.
- [75] R. Ellahi, M. Hassan, and A. Zeeshan, "Shape effects of nanosize particles in Cu- $\text{H}_2\text{O}$  on entropy generation," *International Journal of Heat and Mass Transfer*, vol. 81, pp. 449–456, 2015.



